University of Szeged

Faculty of Pharmacy

Institute of Pharmaceutical Analysis

β-AMINO ACID SUBSTITUTIONS IN β-SANDWICH MODEL PROTEINS

Ph. D. Thesis

Gábor Olajos

Supervisor:

Prof. Dr. Tamás Martinek

2018

Table of Contents

List of publications and lectures

Full papers related to the thesis

I. Olajos, G., Hetényi, A., Wéber, E., Németh, L. J., Szakonyi, Z., Fülöp, F., Martinek, T. A. (2015) Induced folding of protein-sized foldameric β-sandwich models with core β-amino acid residues. *Chemistry – a European Journal*, **21** (16), 6173-6180.

II. Olajos, G., Hetényi, A., Wéber, E., Szögi, T., Fülöp, L., Martinek, T. A. (2018) Peripheral cyclic β-amino acids balance the stability and edge-protection of β-sandwiches. *Organic & Biomolecular Chemistry*, **16**, 5492-5499

Other full papers

I. Mándity, I. M., Wéber, E., Martinek T. A., Olajos, G., Tóth G., Vass, E., Fülöp, F. (2009) Design of Peptidic Foldamer Helices: A Stereochemical Patterning Approach. *Angewandte Chemie International Edition*, **48** (12), 2171-2175

II. Olajos, G., Bartus, É., Schuster, I., Lautner, G., Gyurcsányi, R. E., Szögi, T., Fülöp, L., Martinek, T. A. (2017) Multivalent foldamer-based affinity assay for selective recognition of Aβ oligomers. *Analytica Chimica Acta*, **960**: 131-137

III. Lázár, V., Martins, A,. Spohn, R., Daruka, L., Grézal, G., Fekete, G., Számel, M., Jangir, P. K., Kintses, B., Csörgő, B., Nyerges, Á., Györkei, Á., Kincses, A., Dér, A., Walter, F., Deli, M. A., Urbán, E., Hegedűs, Z., Olajos, G., Méhi, O., Bálint, B., Nagy, I., Martinek, T. A., Papp, B., Pál, C., (2018) Antibiotic-resistant bacteria show widespread collateral sensitivity to antimicrobial peptides. *Nature Microbiology*, **3**: 718-731

IV. Bartus, É., Olajos, G., Schuster, I., Bozsó Z., Deli M. A., Veszelka, S., Fruzsina R. Walter, F. R., Datki, Z. Szakonyi, Z., Martinek, T. A., Fülöp, L., (2018) Structural Optimization of Foldamer-Dendrimer Conjugates as Multivalent Agents against the Toxic Effects of Amyloid Beta Oligomers. *Molecules*, **23** (10), 2523-2536

Scientific lectures related to the thesis

1. G. Olajos, A. Hetényi, T.A. Martinek
   Tervezett β-szendvics foldamerek: egy protein méretű modell
   2014. május 28-30., Peptidkémiai Munkabizottsági Ülés, Balatonszemes

2. G. Olajos, A. Hetényi, E. Wéber, J. L. Németh, T. A. Martinek
   β-sandwich foldamers: A protein sized model
   poster presentation
   7th Central Europe Conference, Chemistry Towards Biology, Katowice
   12-14. September 2014

3. T. A. Martinek, G. Olajos, Z. Hegedüs
   Foladmerek sötét oldala. Béta-redők és szendvicsek
   2018. május 28-30, Peptidkémiai Munkabizottsági Ülés, Balatonszemes

Other lectures

1. G. Olajos, E. Wéber, J. L. Németh, T. A. Martinek
   Designig β-solenoid foldamers: stereochemistry, chain length and hydrophobic packing
   Symposium on Foldamers, Paris,
   12-14 April, 2013

2. R. Nagy, G. Olajos., V. Hársfalvi, Ü. Murvai, R- H. Pires, G. Ferenczy, L. Fülöp, B. Penke, T. A. Martinek, M. S. Kellermayer
   Highly Oriented, Epitaxially Generated Beta-amyloid-based Nanoarray for Nanobiotechnological Applications
   Polymers and Self-assembly: From Biology to Nanomaterials, Rio de Janeiro
   25-30. October 2015

1. G. Olajos, R. Spohn, C. Pál, T. A. Martinek
   Rationally designed antimicrobial foldamers against antibiotic resistance
   9th Central Europe Conference, Chemistry Towards Biology, Budapest
   24-27. September 2018

Abbreviations

ABHC: (1*S*,2*S*,3*R*,5*S*)-2-amino-6,6-dimethylbicyclo[3.1.1]heptane-3-carboxylic acid
ACEC: (1*R*,2*S*)-2-aminocyclohex-3-enecarboxylic acid
ACHC: (1*R*,2*S*)-2-aminocyclohexanecarboxylic acid
ACN: acetonitrile
ACPC: (1*R*,2*S*)-2-aminocyclopentanecarboxylic acid
BB: betabellin
CCA: convex constrain algorithm
CD: circular dichroism
DIPSI: decoupling in the presence of scalar interactions
DMSO: dimethyl sulfoxide
DTT: D,L-dithiothreitol
ESI: electrospray ionization
GB1: B1 domain of protein G from *Streptococcus* bacteria
HATU: 1-[bis(dimethylamino)methylene]-1H-1,2,3-triazolo[4,5-b]pyridinium 3-oxid hexafluorophosphate
HEPES: 4-(2-hydroxyethyl)-1-piperazineethanesulfonic acid
HSQC: heteronuclear single quantum coherence
MS: mass spectrometry
NMR: nuclear magnetic resonance
NOE: nuclear Overhauser effect
NOESY: nuclear Overhauser effect spectroscopy
PPI: protein–protein interaction
RP-HPLC: reversed phase high performance liquid chromatography
SASA: solvent-accessible surface area
Sp1-3: The third zinc finger of specificity factor 1
SSP: secondary structure propensity
TEM: transmission electron microscopy
TFA: trifluoracetic acid
TIS: triisopropylsilane
TOCSY: total correlation spectroscopy

1. Introduction and aims

The function of biological macromolecules, such as DNA, RNA or proteins, depends or their ability to adopt specific, kinetically controlled and thermodynamically stable conformations. This process, referred to as "folding", ensures the precise arrangement of functional groups required for tasks like molecular recognition or catalysis. A similar ability of self-organization is essential for artificial molecules to be capable of mimicking the diverse structural and functional behavior of proteins. The term "foldamer" is used to describe such molecules: artificial polymers with a strong tendency to adopt compact conformations, i.e. **fold**ing poly**mers**.[1, 2]

The first step in the mimicry of complex protein structures is to design stable secondary structural motifs, like helices, β-sheets, and hairpins. A number of foldameric helices, hairpins, as well as several standalone β-sheets were designed, but the cooperative folding of different elements into a tertiary structure is a current challenge, because of the complexity of the problem. The design of water-soluble, stable β-sheets and β-sandwiches is also hindered by their propensity to form insoluble aggregates. Designing stable scaffolds with β-sheet structure is, however, very much desirable, as many aspects of protein functionality are realized through domains with high β-sheet content, like the variable region of antibodies and a great number of protein–protein interaction (PPI) surfaces.[3, 4]

The pharmaceutical need for such protein-mimicking foldamers is also high, because the number of drugs with proteins as active compounds is continuously increasing, but their application is greatly limited, because of their poor pharmacokinetics, stability and immunogenicity.[5] However, many of these disadvantages can be reduced or eliminated by introducing artificial residues into their backbones.

Our goal was to explore the feasibility of β-amino acid substitutions in a complex, protein-sized β-sandwich model. Betabellins, a model protein family were chosen as templates, which are *de novo* designed, 64-residue β-sandwich proteins stabilized by the dimerization of two identical monomeric chains.[6-9] First, we introduced β-amino acid mutations in the hydrophobic core of the β-sandwich to investigate the effects and

tolerability of diverse side chains by using homologous β^3- and conformationally constrained cyclic β-amino acids. We also studied the effect of cyclic β-amino acid substitutions in the peripheral strands of the protein templates with a focus on multiple aspects of structural stability: thermodynamic stability (free energy of reversible unfolding), thermal stability (thermal and cold denaturation), and stability against uncontrolled aggregation.

We employed circular dichroism (CD) spectroscopy to assess the overall and temperature-dependent folding propensity, NMR chemical shift analysis for residue-level structural information, and molecular dynamics calculations for modeling and explaining the side-chain dependent folding behavior. Aggregation tendency was monitored using NMR signal levels and transmission electron microscopy experiments.

2. Literature background

2.1. The mimicry of biological macromolecules

Nature relies on different macromolecules to carry out complex biochemical processes that are needed for life. These sophisticated functions like molecular recognition, catalysis, directing the flow of electrons, or synthetizing other macromolecules require a precise three-dimensional arrangement of functional groups, so they can be carried out only by molecules exhibiting higher-order structure.[10] Nature employs mostly proteins and sometimes RNA for these crucial tasks, as they are unique relative to other biological and synthetic polymers in that they can adopt thermodynamically stable and kinetically controlled conformations.[1]

Successful mimicking the bioactive conformation of proteins is a long-standing goal of chemical science, related to designing inhibitors of protein interactions as well as to understand the principles lying behind the process of acquiring the bioactive conformation, i.e. folding. The term "foldamer" was defined by Gellman to describe any polymer with a strong tendency to adopt a specific compact conformation corresponding to the secondary and tertiary structure of proteins.[1] Protein tertiary structure arises from the assembly of regular secondary structural elements, helices, sheets and turns, thus the first step in the design of foldamers had to be the search for new backbones exhibiting secondary structural preferences. As the peptide bond is a good pillar for noncovalent interactions, many of these new backbones stem from the modification of the natural peptides, like D-peptides, peptoids, β- and γ-peptides, azapeptides, oligoureas, and aromatic oligoamides (Scheme 1).[11]

In a similar fashion to natural self-assembling macromolecules, shape, complementary electrostatic interactions, solvophobic effects, and the formation of H-bonds govern the folding process of non-natural polymers.[1, 12] However, the contribution of the individual interactions and driving forces to the process of self-organization depends on the nature of the building blocks, and thus great diversity can be achieved even at secondary structural level.[11]

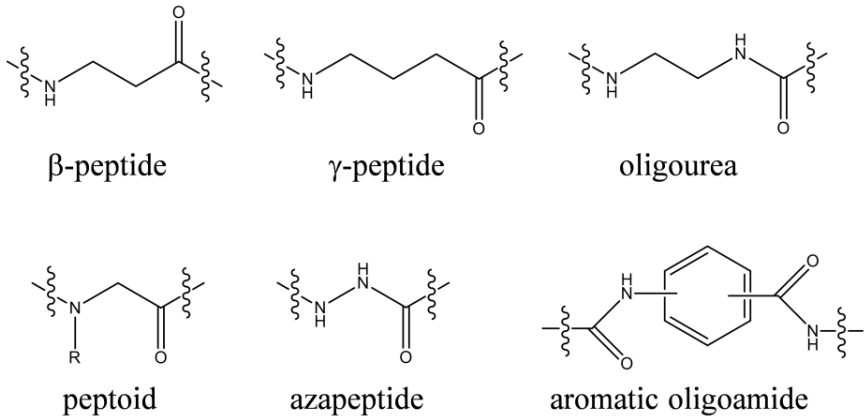

Scheme 1. Representative examples of selected foldameric backbones

2.2.Peptidic foldamers

Closest to the natural peptides are the peptidic foldamers such as β- and γ-peptides, where additional methylene groups are introduced into the backbone between the peptide bonds. Peptidic foldamers can either be constructed exclusively from unnatural building blocks or by mixing natural and unnatural residues to form chimera α/β-, α/γ-, and α/β/γ-foldamers.[13-16] In this case, the H-bonding features of the peptide bonds are retained, and the new carbon atoms introduce an additional substitution position and stereogenic center. This enables the incorporation of proteogenic side chains as well as extending the design space of available residues, thus side-chain interactions – such as solvophobic effects, electrostatic attractions/repulsions and disulfide bridges – can be tailored. The additional carbon atoms in the backbone greatly increase the conformational space, offering a wider range of secondary structural motifs (Figure 1). However, control over the stereochemistry of the backbone also gives a degree of control over the conformational preferences.[17] This also enables the precise orientation of pharmacophore anchor points.

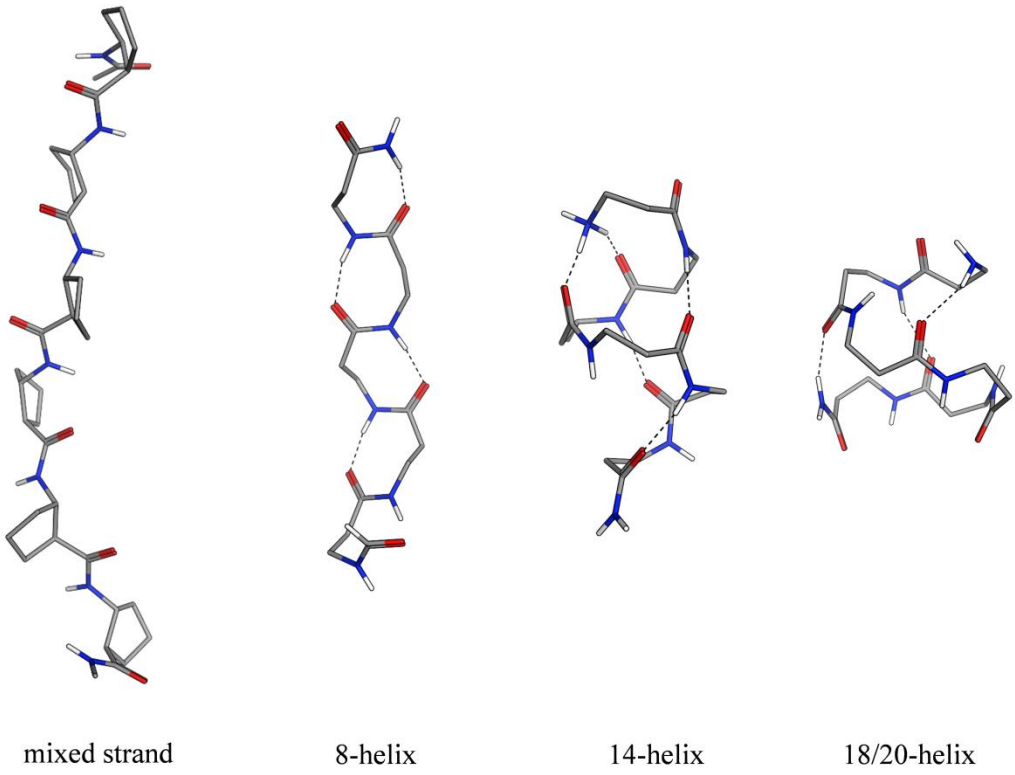

Figure 1. Examples of the diverse β-peptide secondary structures

Peptidic foldamers are also promising alternatives of natural peptides due to their higher folding propensity resulting in stable folds with much shorter sequences than those of α-peptides.[2, 18] Due to shorter chain length, their synthesis, purification and characterization is less challenging compared to antibodies produced by recombinant techniques.[19] Their size is much smaller compared to the average size of antibodies (150 kDa) or even smaller antibody mimetics such as DARPins, aptamers and affibodies (10 kDa); stable fold can be obtained even with foldamers below 1-2 kDa.[20, 21] This feature also enhances the chance of evading immune reactions: it was shown that immune receptors capable of recognizing α-peptidic sequences do not necessarily cross-react with α/β peptide analogs.[22] Another advantage of non-natural peptide sequences is that proteolytic enzymes cannot recognize them, and incorporating β-amino acids in an α-peptide sequence greatly increases stability against proteases; half-life can be 10–20 times longer if 25–30% of the α-residues are replaced.[23-27]

2.2.1. Design of secondary structures

The first step in the mimicry of protein folding is the design of the constituent secondary structural elements. Although the secondary structure of peptidic foldamers is determined by the same principles as of natural peptides – local conformational preferences, hydrogen bonds, electrostatic and hydrophobic interactions –, the rules governing these interactions depend greatly on the backbone and side-chain chemistry of the polymer. An altered backbone particularly affects side-chain conformational restriction, which is the main force to compete with attractive interactions.[28]

Initial approaches were aimed at identifying backbones that favored helical secondary structures, because helices are generally simpler to devise;[1] this is also reflected by the number of soluble helix models in contrast to soluble sheet models. Protein helices are stabilized through a periodical main-chain H-bond network, where nearest-neighbor H-bonding is unfavored.[29] The additional carbon atom offers the possibility to incorporate the amino acid backbones into rings, which gives a high degree of control over the conformational preferences without blocking the H-bonding sites. The rigidified backbone can force the backbone to adopt a favored conformation, inherently promoting the folding process. Homopolimers of *trans*-2-aminocyclohexanecarboxylic acid and *trans*-2-aminocyclopentanecarboxyilc acids were described first, forming 14- and 12-helices, respectively.[30, 31] Open-chain β^3-homologs of proteinogenic amino acids showed also a strong tendency to adopt helical conformation.[32] The shape and H-bond pattern of helices were found to depend on the properties of the residues, and the formation of 8-, 10-, 10/12-, 14/16-, 18 and 18/20-helices has been observed with the introduction of different monomers.[17, 33-36] Chimeric α/β- and α/γ-peptides exhibit even more diverse helix types.[37-39] The analysis of the conformational preferences in helical peptidic foldamers revealed that the signs of the backbone dihedral angles and amide bond orientations are directly controlled by the absolute configuration of the residues. The signs of the torsions flanking the amide bonds are crucial in inducing secondary structures, thus backbone stereochemistry gives

direct control over conformational preferences. This allows the rational design of not only helical scaffolds, but also of extended strands.[17]

The mimicry of the β-sheet secondary structure is less straightforward, as both sheet and turn segments need to be designed into the sequence. The H-bond network of sheets also makes these structures prone to aggregation; hence, suitable capping strategies need to be devised. The standalone constituents of β-sheets, extended strand-like structures, turns and hairpins have been successfully designed,[40-46] but the construction of β-sheets with multiple strands is a great challenge. The side-chain structure of turns can be mimicked with αα→ β^2/β^3 or $\beta^{2,3}$ substitutions, but it was shown that they are not well tolerated in more complex systems.[47] Systematic β^3- and ACHC-substitutions were done in the three-stranded Anginex structure, revealing that lipid-induced folding behavior as well as biologic activity can be retained with peripheral replacements (Figure 2a).[48, 49] Another approach utilized amyloidogenic sequences to promote β-sheet formation while using *N*-methyl amino acids to suppress H-bond formation, thus preventing aggregation. The structure was further stabilized by the formation of a macrocycle (Figure 2b).[50]

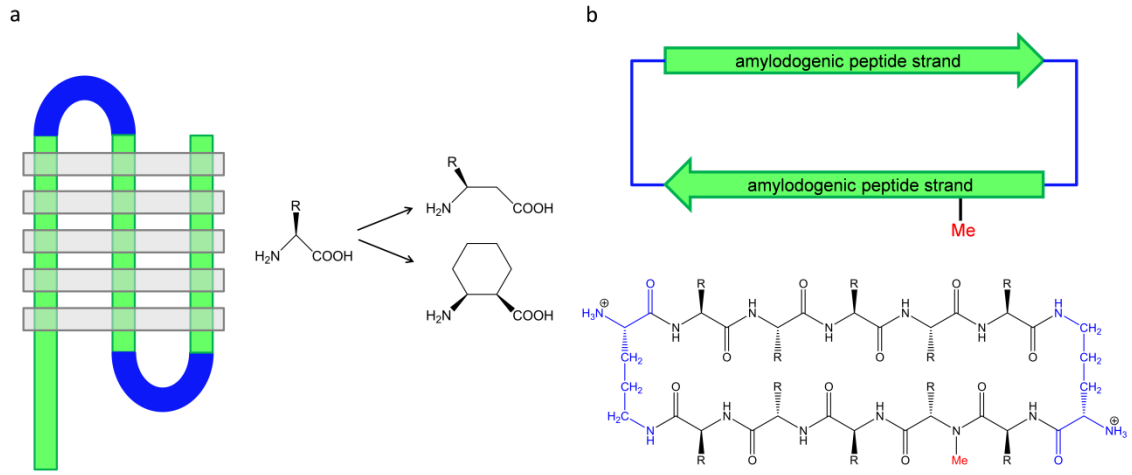

Figure 2. Design strategies for the mimicry of β-sheets. **a)** systematic β^3- and ACHC-replacements in the three-stranded anginex structure. **b)** Macrocycle formed by two amyloidogenic peptide strands; aggregation was suppressed with *N*-methylation.

2.2.2. Design of tertiary and quaternary structures

The design of tertiary structures requires the cooperative interaction of different secondary structural elements. Even if the individual secondary structures have sufficient stability, extending the cooperation to the tertiary and quaternary structural level is challenging. In general, there are two design strategies to construct foldameric structures. If the rules governing the folding process are well established, sequences can be *de novo* designed to fold into the desired conformation. This "bottom-up" approach was utilized to build a great variety of secondary structural elements, but an explicit set of rules for the cooperative folding of tertiary structures is not available. Another approach is to introduce systematic backbone alterations into an existing model system, and to explore the changes in the folding behavior. This "top-down" approach allows the identification of tolerated replacement patterns, and is suitable for the design of larger structures.

One of the simplest higher-ordered structures is the helix bundle, and with stable, rationally designable β-peptide helix scaffolds at hand, the first approaches were aimed towards this quaternary structure. The controlled self-association of an amphiphilic β-peptide helix was shown,[51] while other approaches used disulfide linkage to promote the interactions between the helices.[52] The bottom-up strategy was employed for individual helices to assemble via designed salt-pair and hydrogen-bond interactions, displaying a solvent-excluded hydrophobic core.[53] Natural helix bundles were used as templates for the design of α/β-peptide helix bundles.[54, 55] A systematic study of α/β helix bundles showed that cyclic β-residues are generally well-accommodated in the helix-bundle quaternary structure, but these replacements can be destabilizing in certain instances.[56] Some of the structures exhibited protein-like functions like carbohydrate recognition, metal binding or catalysis.[57]

Linking two helices with a turn segment (helix-turn-helix motif[58]) is another approach toward a tertiary structure, and a single chain that displays cooperative folding is closer to the mimicry of protein-like folding behavior. The first design utilized 15mer peptoid helices with the inherent ability to assemble and used chemical conjugation to construct single-chain 30-, 45- and 60mer helix bundles, which displayed compact structures.[59] A large (>8 kDa) dimeric helix bundle was constructed by linking two

oligoamide helices with an ethylene glycol spacer.[60] Thioester-linked α + α/β helices were used to study the side-chain preferences on the helix interfaces regarding the foldameric subunit.[61] A novel turn-inducing motif (β-hGly-D-Pro-Gly-β-hGly) was used to tether short β-peptide helices with xylose-based side chains, resulting in a stable fold with only 11 residues.[62] An aromatic oligoamide foldamer was recently designed with computational methods to cooperatively fold into a helix-turn-helix tertiary structure, while removal of the turn unit facilitated association into dimeric or trimeric helix bundles.[63]

The mimicry of tertiary structures involving β-sheets was attempted only via the top-down approach. The B1 domain of protein G from *Streptococcus* bacteria (GB1) was presented as a suitable model system, containing both helix, turn and β-sheet secondary elements.[64] Different modification strategies were employed for the different structural motifs, based on observations with secondary structures: homologous β^3-amino acids in the helix, Cα-Me or D-α residues in the turns, and *N*-Me-α residues in the sheet segments (Figure 3a). Though individual modifications destabilized the fold only slightly, and alterations could be combined with near-additive effect on folding energetics, the overall folding of the resulting oligomer was low.[47] Systematic α → β amino acid replacements in the helical segment revealed that replacing α-residues with β-residues enthalpically unfavorable and entropically favorable to the thermodynamic stability of the tertiary fold, and incorporation of cyclic β-residues lower the entropic cost of folding.[65] Diverse backbone modifications were carried out in the strands of the β-sheet involving *N*-methylated α-, vinylogous γ^4-, and cyclically constrained γ-residues (Figure 3b).[66] The study revealed the sensitivity of the hydrophobic core to mutations, as cooperative folding behavior was retained only when the mutations were carried out in the edge strands or next to the turns. The same strategies were used in constructing foldameric analogs of the third zinc finger of specificity protein 1 (Sp1-3, Figure 3c), which were shown to have metal binding affinities comparable or slightly superior to that of the wild type.[67] However, when modifications to the hairpin and helix were combined with alterations to the turns, the resulting variants lost both metal-binding and folding properties. β-Residues of various types have been incorporated into diverse

systems with tertiary folds, including helices in an engineered enzyme,[68] villin headpiece,[69] as well as loops in a vascular endothelial growth factor mimic.[23]

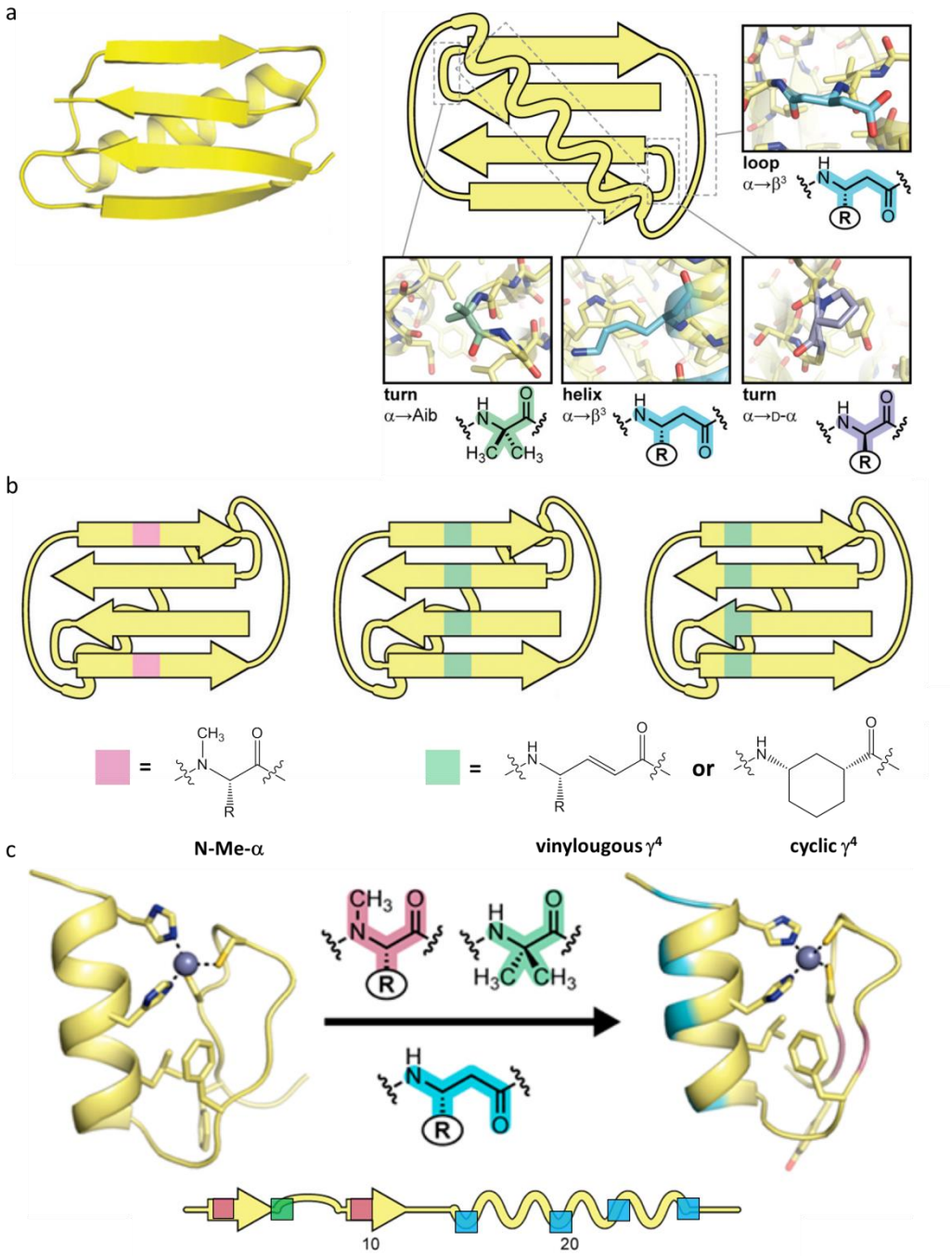

Figure 3. Foldameric tertiary structures involving β-sheets. **a)** Replacement patterns in the model system GB1, with the different residues utilized in each segment.[47] **b)** Modifications of the β-sheet segment in GB1 employing *N*-Me-α and γ-residues. **c)** Design of foldameric analogs of Sp1-3.

2.2.3. Mimicry of protein function with foldamers

Foldamers can be tailored not only to mimic the structural elements of proteins, but to exhibit their characteristic functions, making them a potential tool in the development of novel pharmaceutics. The diversity of proteins makes them capable of carrying out many distinct functions, like catalysis, ion transport or identifying antigens. The basis of these functionalities is molecular recognition, which is essential for interactions to become specific. The surface of foldamers can be designed to recognize different targets, including small molecules, membranes, nucleic acids, and protein interfaces (Figure 4). Selective recognition of diverse small molecules was shown with helical aromatic foldamers termed "molecular apple peels".[70-73] Designed β-peptidic and oligoamide foldamers exhibited DNA-binding properties,[74-77] while different foldamers based on the sequence of the Tat protein displayed high affinity towards the transcriptional activator-responsive element RNA, which is related to the virus HIV-1.[78-81] Membrane-targeting antimicrobial foldamers were designed by mimicking host-defense peptides, as well as for the purpose of cell penetration.[82-87]

Protein–protein interactions (PPI-s) are important pharmaceutical targets, but small molecules were mostly found to be unable to interact with the large and flat surfaces involved in PPI-s.[88, 89] Foldamers have been designed to interact with a wide range of proteins including, but not limited to, different tumor-regulators *h*DM2[90-96] and Bcl-2,[97-101] the HIV-related gp-41,[102-105] targets related to Alzheimer's disease,[106-108] and a number of G protein-coupled receptors.[109-115] The design of these foldamers was based either on the analysis of the protein interaction surface or used the interacting partner as a template. Fragment- and library-based strategies can be employed when only limited structural information is available.

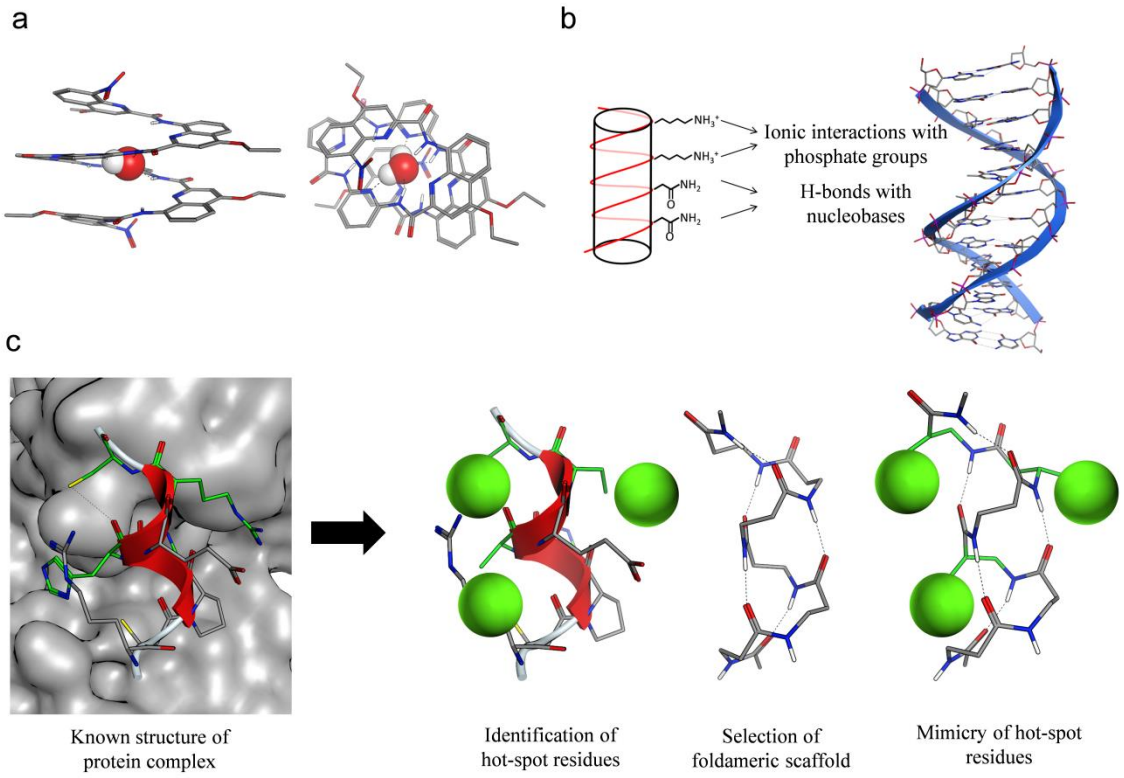

Figure 4. Examples of molecular recognition with foldamers. **a)** Encapsulation of water in an oligoamide helix. **(b)** Design approach of DNA-recognizing β-peptides. **(c)** Protein targeting based on the analysis and mimicry of the hot-spot residues involved in a protein–protein interaction.

2.3. Standalone β-sandwich models

Standalone β-sandwiches are representatives of tertiary structure model systems. The *de novo* design of such systems is very challenging; therefore, only a small number of such constructs have been described in the literature. Computational methods were used to design the sequence of a β-sandwich model peptide called *betadoublet*, which consists of two identical four-stranded β-sheets assembled via disulfide bridge to form a hydrophobic core. The 33mer monomeric sequence was expressed in E. coli and subsequently dimerized. Structure analysis revealed a compact structure with ≈62% β-sheet content and protein-like melting behavior, but it was concluded that truly native-like structure was not present.[116]

The betabellins (BB-s) are a series of 32-residue peptide sequences that have been designed *de novo* to fold into four-stranded β-sheets by virtue of a palindromic pattern with alternating polar and nonpolar side chains and turn-inducing D-amino acids. Their

structure displays a hydrophobic and a polar face upon folding (Figure 5a-b). Hydrophobic effects between the sheets can be enhanced by linking two betabellin monomers with a disulfide bridge through the Cys21 residues resulting in 64-resiude dimeric β-sandwich structures (Figure 5c).[7-9] The different BB sequences displayed various structural behaviors; BB-14 showed no aggregation, whereas BB-15 formed unbranched amyloid-like fibrils and BB-16 formed broad ribbons, both at increased ionic strength. The structures displayed high β-sheet content and protein-like folding behavior, but high-resolution structural data were not obtained because of the transient nature of the fold.

Figure 5. The designed structures and sequences of monomeric betabellin-14 **(a)** and betabellin-15 **(b)**. Residues on the hydrophilic and hydrophobic face are indicated with blue and black, turn-inducing D-residues are indicated with brown, respectively. The proposed structure of betabellin dimers (**c**).

2.4.Stability of proteins

The stability of proteins is a fundamental issue in all biological systems because unfolding usually prevents the biomolecule to carry out its designated role, and in many proteins, the difference in the stability of the folded and the unfolded species is only a few kcal mol^{-1}.[117] The stability must be large enough for the protein to prefer its native conformation over other conformations, but not so high that conformational flexibility is restricted. Rigidity at the strand edges of a protein can result in a conformation rich in misfolded β-sheets leading to uncontrolled aggregation, which in turn is known to initiate various pathological conditions (Figure 6).[118] Aggregation also presents concerns in terms of expressing and purifying proteins and can render biopharmaceutical products unfit for release.[119, 120]

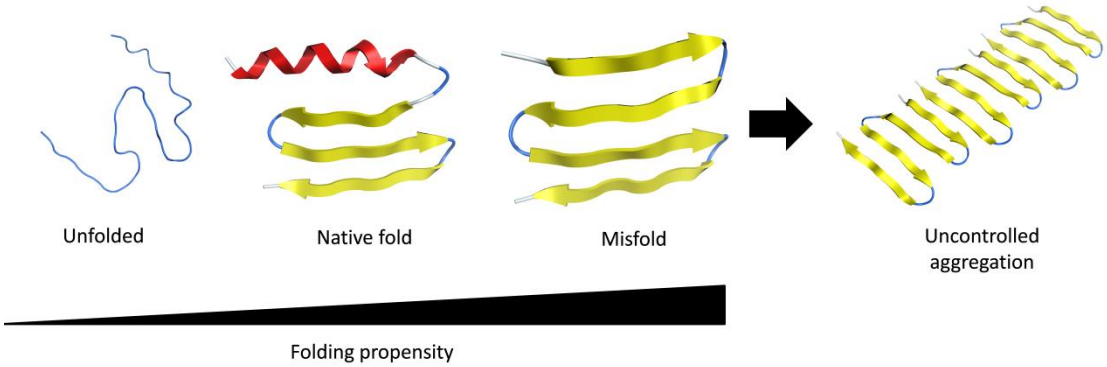

Figure 6. The effect of folding propensity on protein stability. The stability of the fold must be high enough to prefer the natural conformation, but too high β-sheet propensity may lead to aggregation.

The denaturation of proteins due to heat is a clear concept, hence thermal resistance defined by the melting temperature (T_m) is the most often regarded when determining the stability of a protein. Cold denaturation is a property utilized less ferquently, even though it is an inherent property of proteins. The mechanism behind cold denaturation is the entrance of water into the hydrophobic core of the protein resulting from the weakened hydrophobic interactions.[121] Another quantity regarding protein stability is thermodynamic stability, generally defined as the difference in free energy between the folded and unfolded species (ΔG).[122] This quantity can be judged by examining the protein stability curve, which is the free energy of unfolding as a function of temperature.[65, 123, 124] However, calculating the stability curves for a protein under all experimental situations is difficult. The most common techniques to monitor changes in the protein as it unfolds are CD, fluorescence spectroscopy, and NMR. When used to describe protein stability, both T_m and ΔG have shortcomings, but the main problem is that there is a very little correlation between them in a general case. Szyperski et al. have shown that if it is possible to observe both cold and heat denaturation for a given protein, the fitting of the thermogram leads to a reliable determination of the stability curve.[125] A limitation to this method is that cold denaturation is rarely observed in wild-type proteins as most of them exhibit cold denaturation well below water freezing.

In order to prevent edge-to-edge aggregation, natural β-sheet proteins employ negative design elements for edge protection.[126] Some fold types, like β-barrels of β-propellers are protected by the inherent shape of the fold, and β-helices cover their ends with loops. The dominant blocking strategies for single β-sheets and β-sandwiches are

inward-pointing charged residues and different types of β-bulges,[127] which form a protrusion and prevent H-bonding between two edges. Other possible methods are the use of prolines, short strands, and glycines in Lβ conformation.[126] Several artificial edge-protection methods were designed like incorporating *N*-methyl amino acids,[128-130] making a β-bulge by replacing hydrophobic amino acids with lysine[131] or using aromatic β-sheet mimetics.[132]

3. Experimental

3.1. Synthesis and purification of peptides

All materials, except Fmoc-protected ACEC and ABHC, were commercially available. The synthesis and characterization of these building blocks have been described in the literature.[18, 133] Tentagel R RAM resin (0.18–0.2 mmol g^{-1}) was used as the solid support and HATU as the coupling reagent. Couplings were performed by microwave irradiation of an amino acid excess of 3 equivalents at 75 ˚C for 15 min for α-amino acids, and for 30 min for β-residues. Histidine and cysteine were coupled at 50 ˚C. Peptides were cleaved with TFA/H_2O/DTT/TIS (90:5:2.5:2.5), and then precipitated in ice-cold diethyl ether. The resin was washed with acetic acid and water, and subsequently filtered and lyophilized. Peptides were purified by RP-HPLC on a C4 column (Phenomenex Jupiter, 4.6 × 250 mm). The HPLC eluents were (A) 0.1% TFA in water and (B) 0.1% TFA and 80% ACN in water, with a gradient from 25 to 55% B over 60 min at a flow rate of 4 mL min^{-1}. Dimeric peptides were obtained by air oxidation of the purified peptides (5 mg mL^{-1}) in 20% DMSO/water at 37 ˚C for 24 h.[134] The samples were diluted with water and purified analogously to the monomer peptides. Their purity was confirmed by analytical RP-HPLC and ESI-MS measurements.

3.2. Circular dichroism measurements

Circular dichroism measurements were performed by using a Jasco J-815 CD-Spectrometer. CD spectra were recorded by using a thermally jacketed 1 mm quartz cuvette, from 250 to 190 or 195 nm, at a scan speed of 100 nm min^{-1}, with 10 accumulations. Compounds were dissolved in Na-phosphate buffer (pH 6.5), and with peptide concentrations of 100 μM and 50 μM for monomeric and dimeric peptides, respectively. For thermal control, a Julabo water thermostat was used with a 10-min equilibration time at each temperature. The solvent baseline was subtracted. Convex constraint analysis deconvolution of the CD curves was carried out with the CCA+ program.[135-137] In the case of aggregation-prone compounds, the stability of the peptide concentration was monitored via measuring OD at 280 nm with a Shimadzu UV-1800 spectrophotometer.

3.3. NMR experiments

NMR spectra were recorded on a Bruker Avance III 600 MHz spectrometer equipped with a 5-mm CP-TCI triple-resonance cryoprobe at 298 and 308 K. Compounds were dissolved in d_{18}-HEPES buffer (20 mM, pH 6.5) containing 10% D_2O and 0.02% NaN_3. The concentrations of the peptides were 500 μM and 250 μM for monomeric and dimeric peptides, respectively. For referencing, 4,4-dimethyl-4-silapentane-1-sulfonic acid was used as an external standard. Resonance assignment was performed according to the sequential assignment methodology based on 2D homonuclear TOCSY and NOESY. All spectra were acquired with the excitation sculpting solvent suppression pulse scheme with 2048 time domain points and 512 increments. TOCSY measurements were made with homonuclear Hartman–Hahn transfer with a mixing time of 80 ms, using the DIPSI2 sequence for mixing. The number of scans was 16. The NOESY mixing time was 200 ms and the number of scans was 32. For assignment of the ^{13}C resonances, 2D heteronuclear ^{13}C-HSQC spectra were acquired under the same sample conditions as the homonuclear experiments, but the buffer was prepared in D_2O. Processing was performed using Topspin 3.5 (Bruker), a cosine-bell window function, single zero-filling and automatic baseline correction. The spectra were analyzed by Sparky 3.114 (T. D. Goddard and D. G. Kneller, University of California, San Francisco).

SSP scores were calculated using the SSP software.[138] The refDB random coil reference set based on the chemical shifts of properly referenced known protein structures was used. For the dimer structures, the built-in reference set for cysteine residues was replaced with the corresponding values of oxidized cysteine described in the literature.[139] The resonances of the β- and D-α-residues were excluded from the calculations, because of the lack of reference values. Although neighborhood effects of the β- and D-α-residues on the adjacent α-residues cannot be ruled out, our earlier observations demonstrated no major systematic influence preventing the chemical shift analysis.[48, 49]

The salt-dependent aggregation of the compounds was tested by measuring the NMR-visible ^1H signal intensity at various NaCl concentrations; **16** and **18** (Figure 17) were dissolved in the same buffer at a concentration of 250 μM, and the 150-μl samples

were titrated with 1-µl aliquots of a concentrated NaCl solution (3.0 M) resulting in a sample series with NaCl concentrations of 20, 40, 60, 80, 100 and 120 mM. The 1D ^{1}H NMR spectra were acquired for all conditions, and the aliphatic regions were integrated. The integrals were corrected for sample dilution and sensitivity loss caused by high salt concentration with the signal attenuation of a reference sample (2 mM glucose).

3.4. Transmission electron microscopy

250 µM solution of the peptide in phosphate buffer (20 mM, pH 6.5) containing 150 mM NaCl was placed on formvar-carbon-coated 400-mesh copper grids (Electron Microscopy Sciences, Washington, PA) and stained negatively with uranyl acetate. The aggregates were characterized by TEM on a JEOL JEM-1400 transmission electron microscope (JEOL USA Inc., MA, USA) operating at 120 kV. Images were taken with EM-15300SXV, SightX Viewer Software (JEOL) routinely at magnification of ×25000.

3.5. Molecular modeling

Molecular structures of the peptides were generated with Schrödinger's Maestro and CCG's MOE. The folded β-sheets were aligned according to the facing reported for betabellin-14.[6] Molecular dynamics simulations were run using the GROMACS molecular dynamics software with the AMBER ff03 force field extended to β-amino acids.[140] The peptides were solvated in a cubic box using TIP3P explicit solvent model. The net charge of the peptides was neutralized by adding Cl^{-} counter ions. The energy was minimized using the steepest descent algorithm. The system was then heated to 300 K during a 100 ps constant volume simulation with 1 fs time step. The pressure was then equilibrated to 1 atm during a 100 ps NPT simulation with 2 fs time step. Production runs were 150 ns simulations for all sequences with a step size of 2 fs. Temperature coupling was done with V-rescale algorithm. Pressure coupling was done with the Parinello–Rahman algorithm. The structures were clustered with the gromoss method using 0.1 nm cutoff for alpha carbon RMSD.[141] Average solvent-accessible surface area (SASA) was calculated through the trajectory for each residue. The maximum allowed SASA values for amino acids were calculated using Gly-Xxx-Gly tripeptides as a host-guest system. Solvent exposure was calculated as the fraction of the

folded and the maximum surface area of each residue. The presence of hydrogen bonds was determined with 0.35 nm cutoff radius and 30° cutoff angle.

4. Results and discussion

4.1. Core β-amino acid mutations in the β-sandwich model protein betabellin-14

4.1.1. Design approach

In order to study the folding behavior of a protein-sized foldameric scaffold, we intended to use a top-down approach by using a suitable β-sandwich model protein as template and introduce β-amino acid mutations into its sequence. Betabellin-14 (BB-14) consists of a 32-residue palindromic pattern of polar (p), nonpolar (n), end (e), and turn (t, r) residues (Figure 7a). When β-turns are induced with D-Lys-D-Ala (tt) and D-Ala-D-Lys (rr) segments, the sequence tends to fold into a four-stranded amphiphilic β-sheet.[9] The hydrophobic interactions can be enhanced by linking two betabellin chains through a disulfide bridge involving the Cys21 residues. This enforces the intermolecular interactions between the sheets and promotes β-sheet formation. The resulting 64-residue β-sandwich is the size of a small protein, and shows protein-like structural behavior. BB-14 was selected as template for two reasons: i) its high water-solubility suggested low or no aggregation propensity, and ii) its folding greatly depends on dimerization, which facilitated the study of the effects of mutations on the inducibility of the folding. For the β-amino acid substitutions, we chose residues *I12* and *A19* as mutation points on the hydrophobic face of the β-sandwich, as these core substitutions may have a major effect on the folding process. These residues are situated in isolated positions to let the β-residues accommodate their local environment and to minimize the interaction and steric clash between the substituted amino acids (Figure 7b). We found earlier that β^3-residues with large hydrophobic side chains tend to attain a gauche backbone conformation in a β-sheet environment, but no studies were carried out in a hydrophobic core isolated from the solvent.[48] To test the effects of the conformational constraints, we also synthetized analogs containing cyclic β-amino acids. In accordance with the rules of the stereochemical patterning approach, *cis*-backbone arrangement (with configurations of *R* and *S* at the α- and β-carbons, respectively) was applied for

the optimized interstrand H-bond network. It was demonstrated previously that a steric clash between bulky side chains can exert a major influence on the secondary structure, because the hydrophobic core is only stable – shielded from the solvent – if the side chains are tightly packed.[35] This means that the steric fit of the side chains is another important factor to optimize; therefore, we selected cyclic β-residues with various steric requirements (Figure 7a): (1*R*,2*S*)-2-aminocyclopentanecarboxylic acid (ACPC), (1*R*,2*S*)-2-aminocyclohexanecarboxylic acid (ACHC), (1*R*,2*S*)-2-aminocyclohex-3-enecarboxylic acid (ACEC) and (1*S*,2*S*,3*R*,5*S*)-2-amino-6,6-dimethylbicyclo[3.1.1]-heptane-3-carboxylic acid (ABHC).

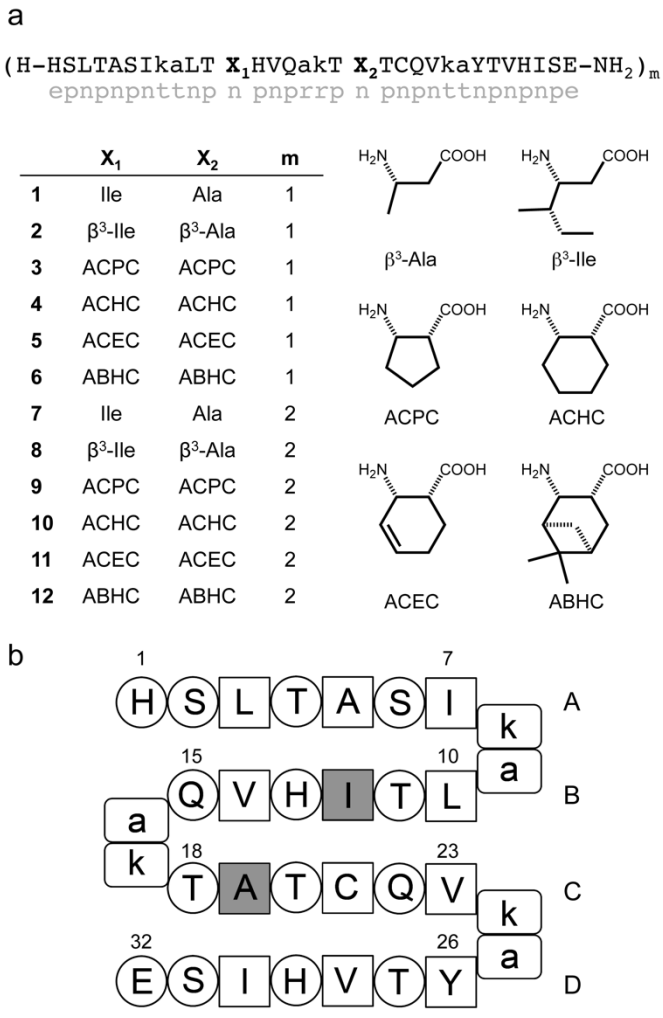

Figure 7. The amino acid sequence and palindromic design (gray) of the betabellin-14 analogs studied (**a**). Residues are coded with the standard one-letter α-amino acid notation; lower-case letters indicate D-α-amino acids. Schematic representation of the β-sandwich fold of the betabellin-14 monomer with the

selected positions for the mutations (highlighted in gray) (**b**). Constituent strand segments are designated by capital letters A–D.

4.1.2. Dimerization-induced β-sheet formation

We used CD spectroscopy to monitor the overall propensity of the betabellin-14 analogs to attain a specific secondary structure. The possible effects of β-amino acid substitutions on CD signals were not exactly known *a priori*. However, the analogs contain only 6.25% β-residues and, therefore, the CD curves were expected to resemble those of natural peptide sequences. The experimental conditions were chosen so that the solubility of the peptides was maintained and the background absorbance and noise were kept low. Therefore, experiments were carried out in Na-phosphate buffer at pH 6.5 using a peptide concentration of 100 μM for the monomeric compounds, and 50 μM for the dimeric compounds so that the absorbances were at the same level.

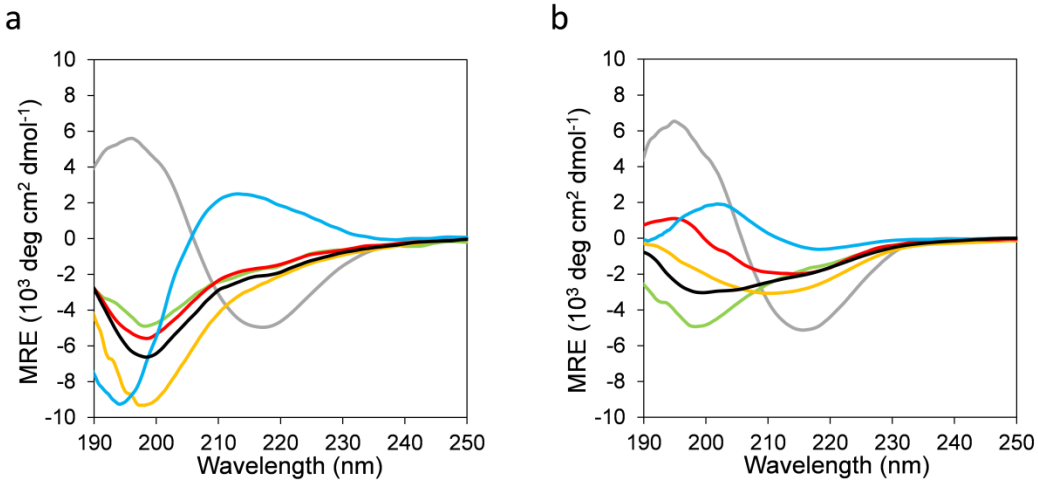

Figure 8. a) Mean residue ellipticities (MRE) obtained for monomeric betabellin-14 (**1**) and the α/β-peptidic analogs **2**–**6**, indicated in gray, green, yellow, red, blue, and black, respectively. **b)** MRE curves obtained for dimeric betabellin-14 (**7**) and α/β-peptidic analogs **8**–**12**, indicated in gray, green, yellow, red, blue, and black, respectively.

The spectra recorded for the parent sequences **1** and **7** were in accordance with literature observations, although the characteristic CD curve of the β-sheet was observed in the monomeric form already (Figure 8a), but dimerization through the disulfide bridge further increased the β-sheet content. The α/β-analogs **2**–**4** and **6** yielded distorted U-shaped CD curves with an intense negative band at around 199 nm, and a lower-intensity band at around 220 nm, suggesting mostly disordered

conformations (Figure 8a). Dimerization resulted in marked changes in CD responses: the negative band disappeared or became less dominant for all sequences (Figure 8b). The ACEC-containing analogs displayed contrasting CD spectra: a positive Cotton effect was observed for **5**, whereas **11** exhibited inversion and an intensity decrease. This could be explained in terms of the exciton coupling to the side-chain double bond, based on similar anomalous CD behavior observed earlier for helical β-peptide foldamers containing the ACEC residue.[18] Overall, these changes suggested formation of ordered conformational states upon dimerization.

A CD spectrum is the weighted sum of the component spectra of the secondary structure elements, and the curves observed are, therefore, very sensitive to the conformational ensemble, and visual inspection may be misleading. In order to extract quantitative information, a convex constraint analysis deconvolution[135] was carried out simultaneously on all spectra recorded for this study, with the exceptions of those recorded for the peptides containing ACEC building blocks (**5** and **11**). This approach calculated the pure component spectra and their weights without making use of any input basis spectrum or structural hypothesis. The normalized residual mean square deviation between the fitted and the experimental curves averaged over all included compounds was 3.94%, which indicated acceptably low fitting error. The protocol produced three spectra as base components (Figure 9a), to which we assigned secondary structural elements based on their similarity to reference CD curves of pure secondary structures.[142] The first component exhibited a minimum around 217 nm resembling the characteristic CD curve of β-sheets. The second component had a minimum around 195 and was assigned as the disordered conformation. Assigning the third component was less straightforward: we determined it as the contribution of β-turns formed by the D-α-amino acids.[136] The corresponding coefficients estimated the contributions of the components, and so the percentages of the secondary structure content were obtained (Figure 9b). The β-sheet content of the parent α-peptide sequences (**1** and **7**) changed from 43% to 67% upon dimerization indicating the stabilizing effect of the enhanced hydrophobic interactions in the disulfide-stabilized β-sandwich.

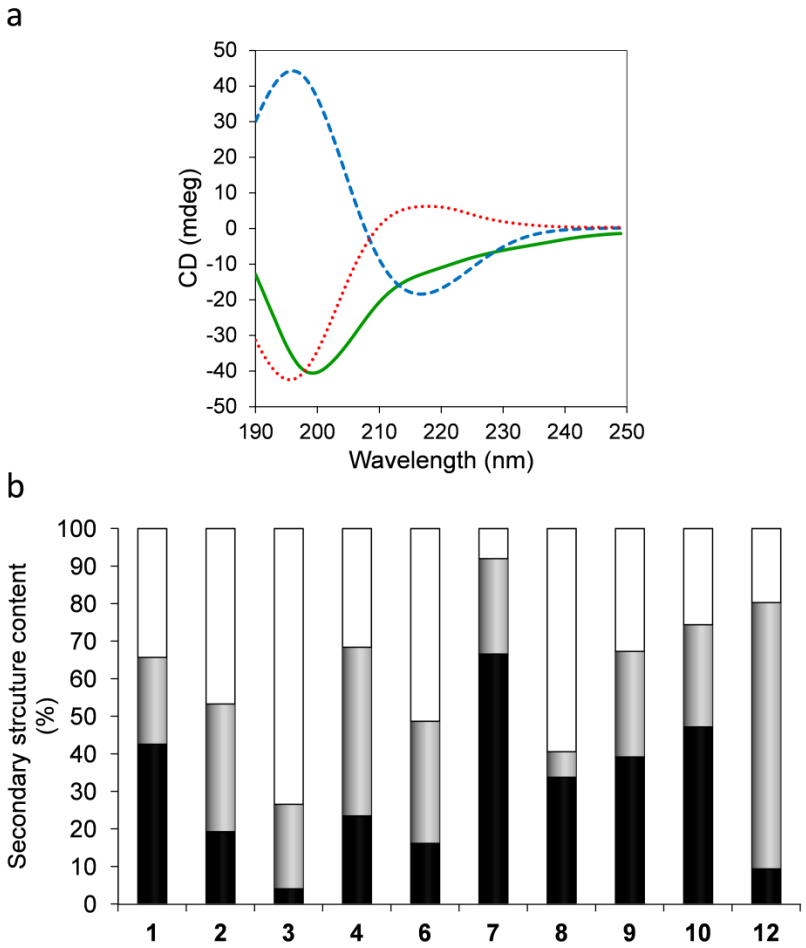

Figure 9. a) The three pure components of the CD spectra calculated by convex constraint analysis algorithm. Secondary structure elements: disordered (red dotted), β-turn (green solid), β-sheet (blue dashed). **b)** Secondary structure contents calculated by using the convex constraint analysis algorithm for the CD curve deconvolution. β-sheet, β-turn, and disordered components are indicated in black, gray, and white, respectively.

The analysis revealed that the α/β-peptides are mainly disordered in the monomeric form, and the β-sheet content varied in the range of 4–24%. On the other hand, the dimerization increased the β-sheet ratio to the range of 34–47% for **8**–**10**. In both cases, the highest β-sheet ratio was observed for the analog containing ACHC building blocks (**4** and **10**). In contrast, the sequence containing the bulky ABHC residues (**12**) indicated a decrease of β-sheet content after disulfide bridge formation, pointing to the presence of a steric clash. The β-turn contents for **1** and **7** were found to be 23% and 25%, which were in line with the nine residues forming the three-turn structures (28%). The closest ratios to these reference values were observed for **9** (28%) and **10** (27%), whereas **8** and

12 displayed marked deviations. These findings supported our hypothesis that, despite the destructuring effects of the β-residue mutations, β-sheet formation remains inducible, if the hydrophobic interactions are at least partially maintained. In this case, the stabilization effects of the forced β-sandwich formation proposed originally for betabellin-14 were able to push the α/β-sequences toward the β-sheet fold.

4.1.3. Structural propensity at the residue level

The chemical shifts of the backbone nuclei depend on the dihedral angles ψ and φ that is they are affected by the secondary structure.[143] NH, H_α, C_β and N chemical shifts exhibit a downfield shift, whereas C_α chemical shifts exhibit an upfield shift relative to a disordered reference upon β-sheet formation and the opposite change is observed for helices.[144] The difference between the experimentally determined and a set of random coil chemical shifts ($\delta - \delta^{rc}$) defines secondary chemical shifts, which can be used to detect transiently formed secondary structures.[145-147] Homo- and heteronuclear NMR spectra were recorded and assigned for the monomeric and dimeric sequences in natural abundance under optimized conditions (HEPES buffer, 500 μM, 298 K) (Figure 10). Homonuclear TOCSY and NOESY spectra were used to assign NH and H_α chemical shifts, heteronuclear ^{13}C and ^{15}N HSQC to assign C_α and C_β and N chemical shifts. ^{13}C HSQC was measured in pure D_2O with identical buffer composition in order to assign C_α chemical shifts by eliminating the water signal. In this way, the majority of the chemical shifts were assigned except for NH and N chemical shifts for His1 and Ser2. All identified $^{1}H_\alpha$, ^{1}HN, $^{13}C_\alpha$, $^{13}C_\beta$ and ^{15}N resonances were included in the secondary chemical shift analysis. The set of secondary chemical shifts was combined into the secondary structure propensity (SSP) score, which was calculated by using the ssp software.[148] This score gives a semiquantitative measure of the residue-level secondary structure distribution along the chains. The resonances of the β- and D-α-residues were excluded from the calculations, because of the lack of reference values. Although secondary structure-independent neighborhood effects of the β- and D-α-residues on the magnetic environment of the adjacent L-α-residues cannot be ruled out, our earlier

observations indicated no major systematic influence preventing an analysis of the secondary structure trends.[48]

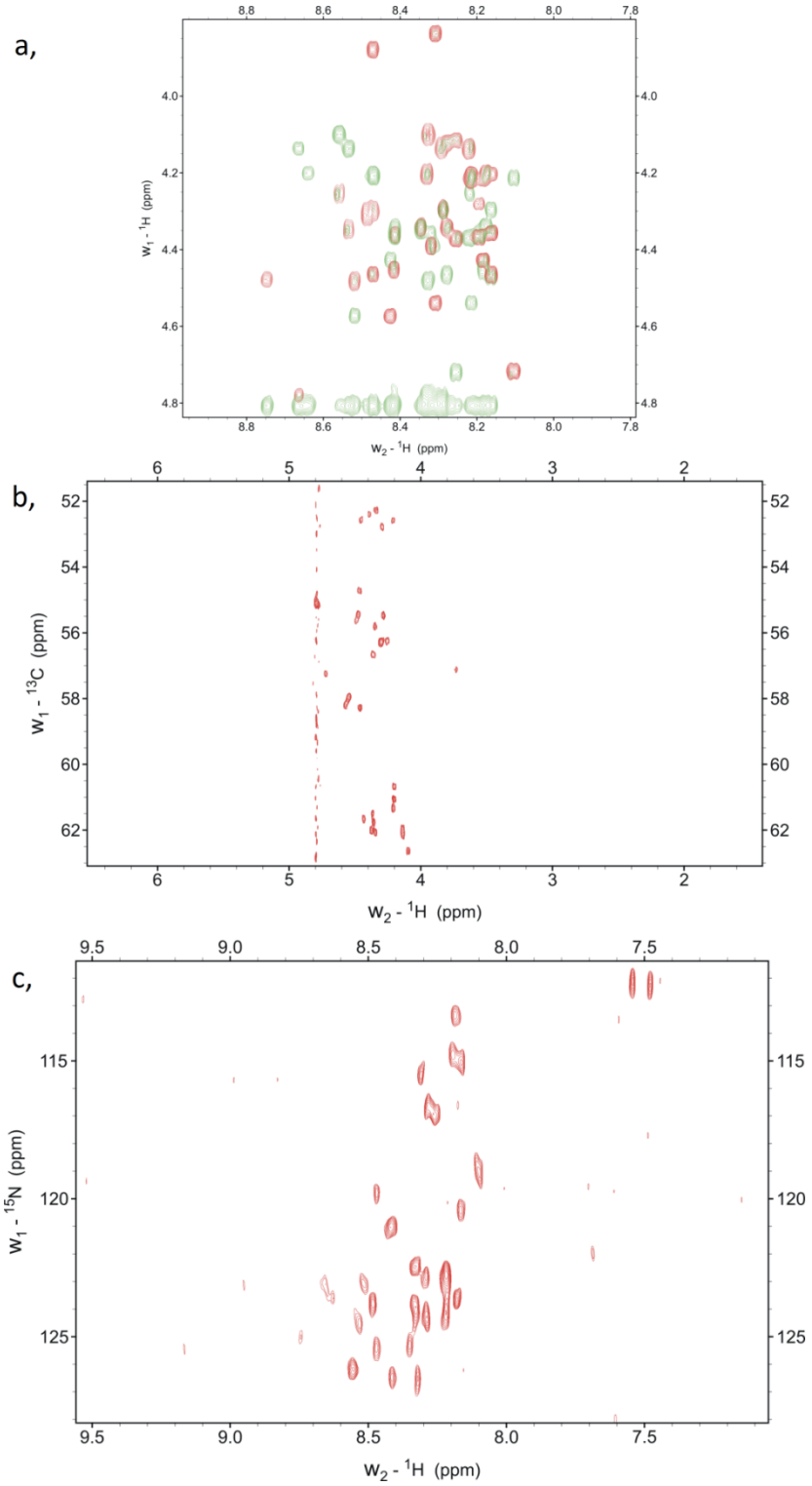

Figure 10. Representative NMR spectra of **1**. The full set of spectra can be found in the supporting data of the original article, DOI: 10.1002/chem.201405581

The set of negative SSP scores obtained for the monomeric parent sequence **1** was a good indicator of the β-sheet tendency in line with the CD results (Figure 11a, grey). The largest β-sheet content was found in segment B. As seen in the CD spectra, dimerization through disulfide formation in **7** increased the β-sheet content, which is displayed in the decreased SSP scores along the chain (Figure 11b, grey). The change in β-sheet propensity was the most pronounced in strand C containing the tethering Cys_2 residues, and propagated to strands B and D. This indicated that the forced hydrophobic interactions are effective at stabilizing the core of the β-sandwich. The residue-level results also confirmed betabellin-14 as a useful inducible β-sandwich model. For monomeric analogs **2**–**6**, the SSP score increase around the β-residues (positions 12 and 19) reflected the local disorder caused by these mutations, supporting the CD findings. The destructuring pattern of the β-residues was also observed for the dimeric α/β-peptides **8**–**12**, but the disulfide bridge increased the β-sheet content in segment C up to the values observed in segment B. This enhancement effect was side-chain-dependent.

In order to study the dimerization-induced structural changes, we calculated the differences in the SSP scores of the monomeric and dimeric compounds (Figure 11c). This representation eliminated the influence of the reference chemical shifts and the data depict the dimerization-induced β-sheet enhancement along the sequences as concerns the L-α-residues. For the β-turns of the D-α-residues, secondary structure type changes cannot be directly assigned to the values, but the ΔSSP scores can be compared with those for the parent sequences. It is clear from this analysis that the dimerization-induced β-sheet enhancements are present for the α/β-sequences except for the ABHC-containing sequence **12**, which displayed similar behavior in the CD experiments. Interestingly, the largest increases were observed in the proximity of the β-residues in position 19, indicating the inherent ability of the β-residues to fit into a β-sheet environment if extra stabilization is introduced. The best results were obtained with derivative **10**, which displayed ΔSSP scores in segment C similar to those for the parent sequence. The residue-level β-sheet enhancements, however, were mostly located at the tethered segment C in the α/β-analogs, which suggested that the propagation of the

stabilization effects to the neighboring strands was less efficient as compared with **7**. These results suggested that side-chain bulkiness and the preferred arrangement of backbone torsions at the β-residues had profound effects on the β-sheet packing and, thereby, on the stabilization of the fold. The residual flexibility of this sensitive system and the signal overlaps in the 2D ^{1}H-homonuclear spectra did not permit the assignment of diagnostic NOE interactions. We also attempted to crystallize **7** and **10** to obtain high-resolution structural data via X-ray crystallography, but none of the conditions tested resulted in suitable crystals.

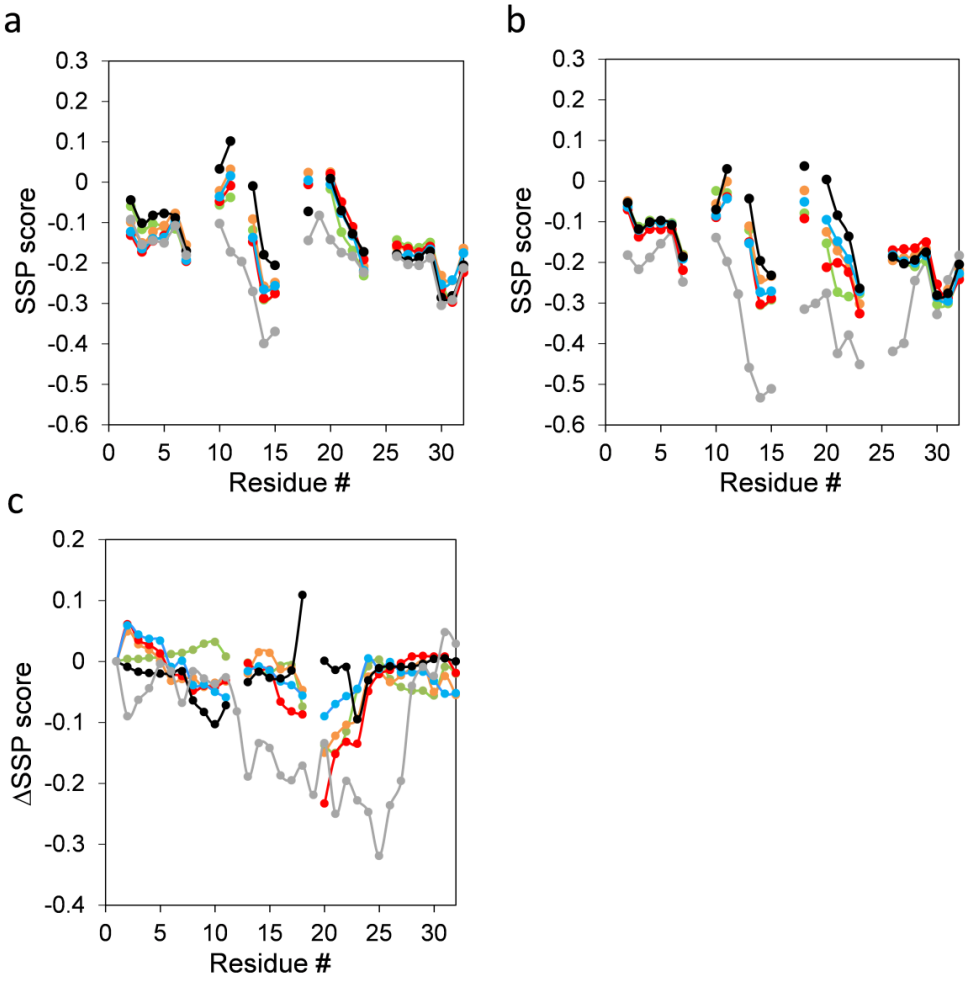

Figure 11. Residue-level secondary structure propensity (SSP) scores calculated on the basis of the $^{1}H_{\alpha}$, ^{1}HN, $^{13}C_{\alpha}$, $^{13}C_{\beta}$ and ^{15}N NMR chemical shifts. SSP scores obtained for monomeric BB-14 (**1**) and α/β-peptidic analogs (**2**–**6**), indicated in gray, green, orange, red, blue, and black, respectively (**a**). SSP scores measured for dimeric BB-14 (**7**) and α/β-peptidic analogs (**8**–**12**), indicated in gray, green, orange, red, blue, and black, respectively (**b**). SSP score differences including D-α-residues obtained upon dimerization (**c**) are color-coded by using the same scheme as given in panels (**a**) and (**b**). Difference values hold structural meaning only for the L-α-residues.

4.1.4. Thermal stability

The presence of secondary structural elements can be assessed using CD and NMR responses, but the mimicry of protein-like folding behavior also requires the cooperative assembly of the structure components. A certain amount of rigidity is required for a stable fold, which is sensitive to denaturation either due to heat or cold as seen in well-folded proteins. This is possible if the residual flexibility of the folded system is sufficiently low, the stabilization is driven by a well-packed hydrophobic core, and the H-bond network is mostly complete.[149] Temperature-dependent CD measurements described in the literature revealed that dimeric BB-14 undergoes thermal denaturation with a melting temperature T_m of 58 °C.[9] This phenomenon could be reproduced for **7**, but in our hands, the Na-phosphate buffer (pH 6.5) shifted T_m to 50 °C (Figure 12a and f). Together with the cold denaturation observed below 25 °C, these findings supported the view that **7** is stabilized by hydrophobic contacts between residues remote in the sequence, and the thermal unfolding is cooperative, due to the tightly packed hydrophobic cluster of the β-sandwich fold. The analysis was performed for the dimeric α/β-analogs apart from **11**, where the shape of the CD curve was affected by the side-chain exciton coupling. We found that a thermal denaturation feature similar to that for **7** could be observed only for **10**, the ACHC-containing analog, and cold denaturation was observed as well (Figure 12d and f). Temperature-dependent increase in the β-sheet content was seen for sequences **8**, **9** and **12**, but the thermal unfolding phenomenon could not be captured. This can be explained by the temperature dependence of the hydrophobic interactions, but no denaturation takes place as the structures are not stable enough to begin with. These findings suggest that the ACHC building block in **10** has the structural features (local conformational preferences and side-chain shape) that are required to maintain sufficient compactness and rigidity of the β-sandwich fold, which mimics proteins. On the other hand, the other tested β-residues were not able to reach this limit.

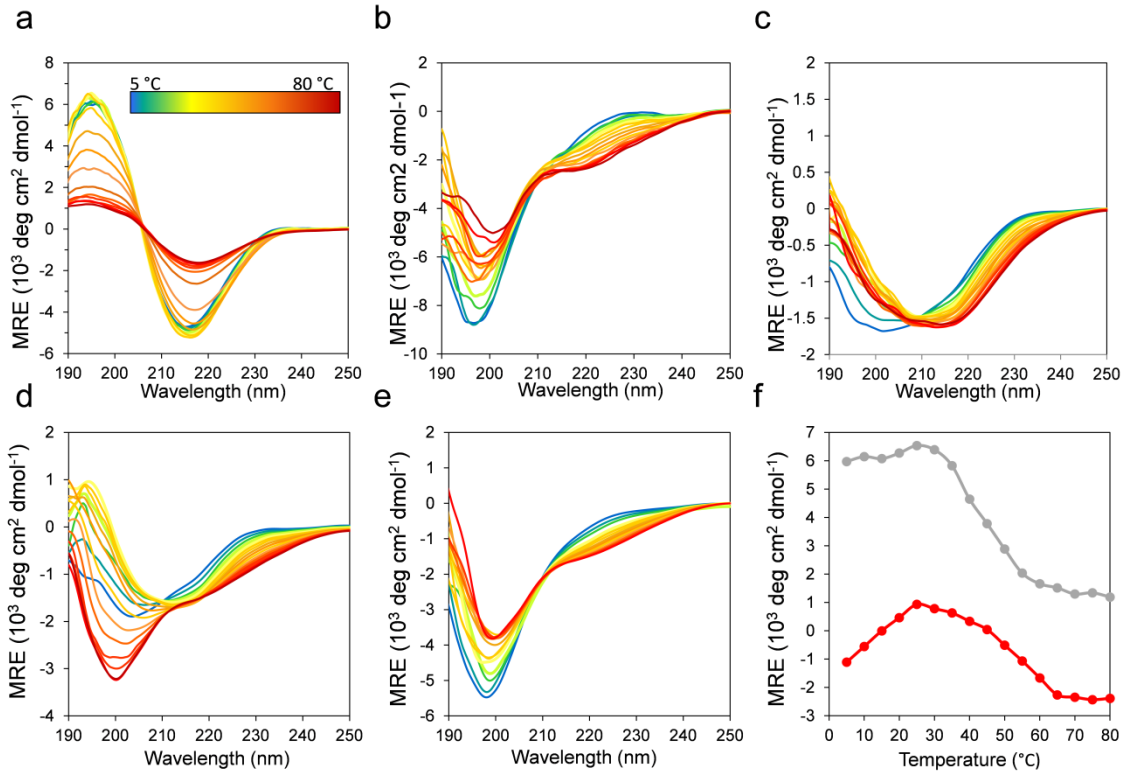

Figure 12. Temperature-dependent CD curves recorded for **7**–**10** and **12** depicted in panels (**a**)–(**e**), respectively. The color code for the temperature scale is given as panel (**a**). MRE values at 195 nm for **7** (grey) and **10** (red) (**f**)

4.1.5. Effect of β-residues on the β-sandwich packing

In order to find explanation for the side-chain-dependent folding behavior, molecular dynamics calculations were run for the dimeric sequences **7**–**12**. The modeling was based on the AMBER ff03 – TIP3P force field combination, which has been validated for the modeling of β-peptidic sequences in water.[140] The initial β-sandwich geometry for the calculation was the structure proposed in the literature for the betabellin family.[6] We performed preliminary calculations with various intersheet orientations to confirm the proper orientation and found that the published geometry provided the lowest solvent-accessible surface area for the hydrophobic core. Thus, simulations were started from the proposed β-sandwich fold, and the conformational space was sampled for 150 ns. Since the α/β-analogs were expected to change their overall conformations relative to the parent sequence and to display increased flexibility, the convergence of the simulations was monitored by the rate of

conformational cluster formation. We have found that the number of clusters reached a plateau within the time span of the modeling, which was indicative of the acceptable sampling of the conformational ensembles. The results obtained with sequence **7** were in close correlation with experimental observations. Inspection of the lowest-energy structures of **7** confirmed the target β-sandwich fold with a compact hydrophobic core (Figure 13a). The number of clusters calculated over the trajectory was 82, as the fraying terminal introduced a degree of flexibility, which was expected from the experimental results. For α/β-analogs **8**–**12**, the number of clusters was 735, 751, 192, 430 and 414, respectively, which indicated a marked increase in flexibility relative to **7**.

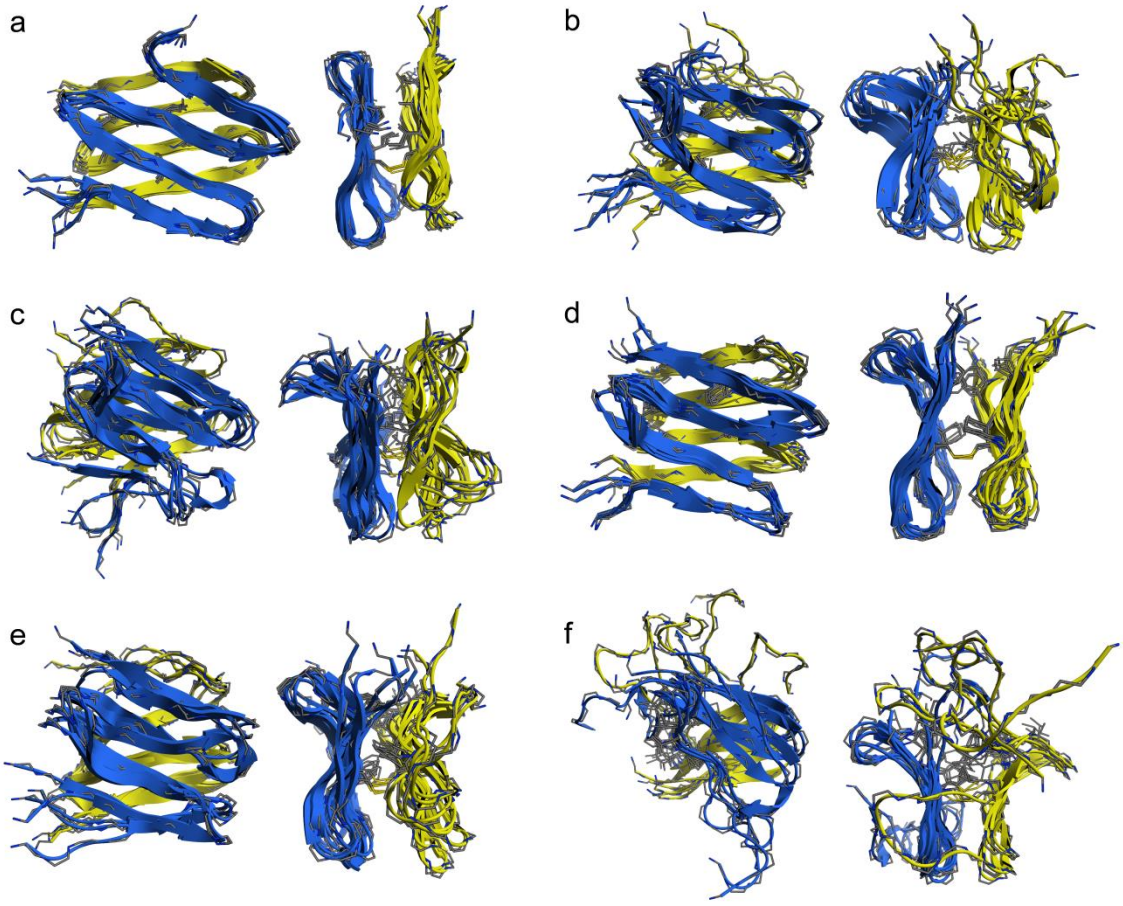

Figure 13. Overlay of the five lowest-energy structures obtained in molecular dynamics simulations for sequences **7**–**12** in panels (**a**)–(**f**), respectively.

Nevertheless, **10** was predicted as the most rigid sequence among the α/β-peptides, which fell completely in line with the CD and NMR results. Comparison of the lowest-energy structures with that of **7** revealed that the β-residue mutations not only increased

the flexibility, but also changed the overall shape of the constituent β-sheets. This deviation from the compact β-sandwich fold was the lowest for **10** (Figures 13d and 14a), yielding the best compactness of the hydrophobic core (Figure 14b) and the highest ability to maintain the H-bonding network (Figures 14c and d). In the low-energy conformations, it was possible for the ACHC residues to form all the local backbone H-bonds, while the steric packing of the β-sandwich interior was at an acceptable level (Figure 15).

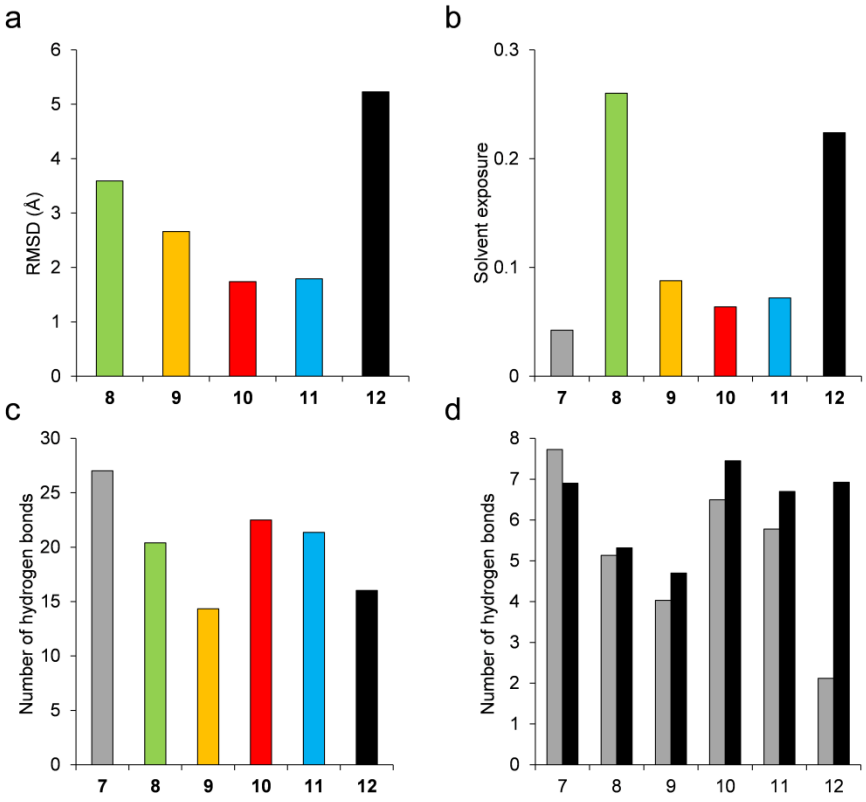

Figure 14. Root mean square deviation (RMSD) of lowest-energy structures from the parent β-sandwich fold **7** (**a**). Average solvent-exposure ratio of the core hydrophobic residues in strands B and C (**b**). The number of existing H-bonds in the β-sheets (theoretical maximum: 36) (**c**). The number of H-bonds observed for the residues in positions 12 (gray) and 19 (black) (theoretical maximum: 8) (**d**).

These results were also in accord with the experimental data. In the case of **8**, the solvent accessibility of the core residues greatly increased and the H-bonding network was disrupted (Figure 14b and c). The analysis of the structures revealed that the reason behind this is that the β^3-residues introduced an overall curvature into the β-sheet and increased conformational flexibility. Interestingly, ACPC residues in **9** obtained a degree of core shielding comparable to that of **10**, but its ability to form H-bonds in the

β-sheet environment was the worst among the β-residues. ACEC (**11**) was able to produce low-energy structures and a level of core compactness similar to those of **10**, but its fit into the H-bonding network was less successful, as indicated by the diminished number of H-bonds around the β-residue. This may be attributed to the effects of double bond on the ring constraint, which determines the dihedral preferences of the backbone. Sequence **12** mostly unfolded over the simulation trajectory, due to the steric repulsion interactions between the bulky side chains. The lowest-energy structures retained the β-sheets only partially, which resulted in solvent-exposed hydrophobic residues and missing H-bonding network on one side of the β-sandwich.

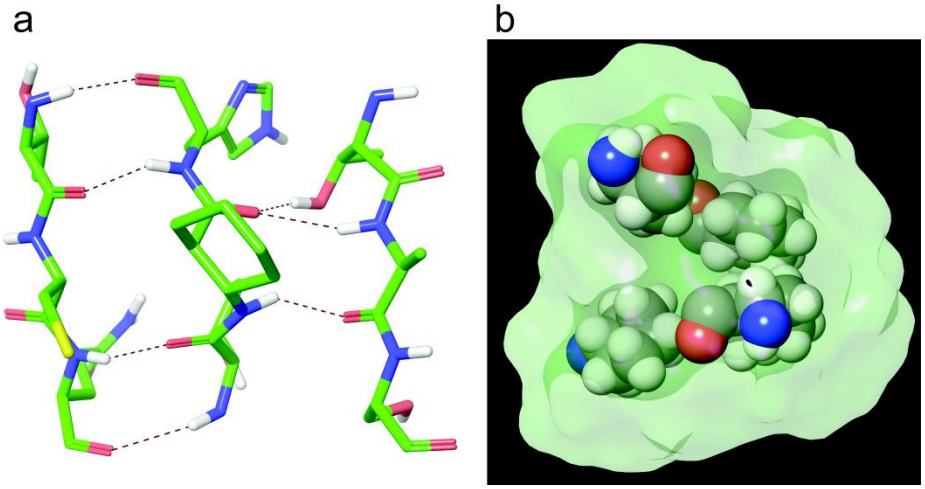

Figure 15. a) The H-bond network around the ACHC12 residue in a representative low-energy structure of **10**. **b)** Steric fit of the ACHC residues (van der Waals spheres) into the hydrophobic interior of the β-sandwich (shaded volume) in a representative low-energy structure of **10**.

These findings correlated well with CD and NMR results. We found that a reduced number of H-bonds were formed in time average around the β-residues, even if the side-chain size matched those of the replaced α-residues. This could explain the reduced β-sheet tendency and lateral propagation of order upon β-sheet dimerization. The overall stability of the β-sandwich fold, however, was influenced by the residue properties in a complex manner. These simulations suggested that local conformational fit into the β-sheet geometry and the compatibility with the hydrophobic core of the β-sandwich were equally important. For example, the β^3-residues displayed a reduced state of compactness around the side chains, but the backbone flexibility afforded relatively

good contacts to the H-bonding network. In contrast, ACPC set well in the hydrophobic interior, whereas the local conformational preferences reduced the number of H-bonds. ABHC residues provided an extreme case, where the steric clash between the side chains prevented the formation of the solvent-shielded β-sandwich core, thereby leading to unfolding, despite the fact that the backbone conformation was fixed and it was the same as that for ACHC. The fit into the β-sheet strands and into the hydrophobic core were simultaneously the best for ACHC among the β-residues. This resulted in considerable β-sheet content, inducibility of the structure, and protein-like thermal unfolding behavior.

4.2. Balancing edge protection and stability of model proteins with peripheral ACHC-substitutions

4.2.1. Design approach

According to our results with core *cis*-ACHC-substitutions, this residue is able to accommodate to the β-sheet environment well enough to maintain considerable β-sheet content and protein-like folding behavior. However, both SSP scores and modeling results pointed out a local distorting effect of the β-residues, resulting in the formation of a bulge in the strands (Figure 16). As β-bulges are among the most common natural strategies to prevent edge-to-edge aggregation,[126, 127] we intended to investigate the possibility of introducing peripheral bulges via *cis*-ACHC-mutations to reduce aggregation propensity.

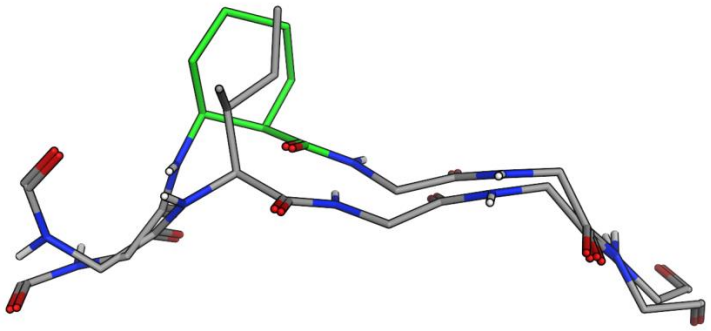

Figure 16. The β-bulge introduced by the *cis*-ACHC13 residue (green) in **10**.

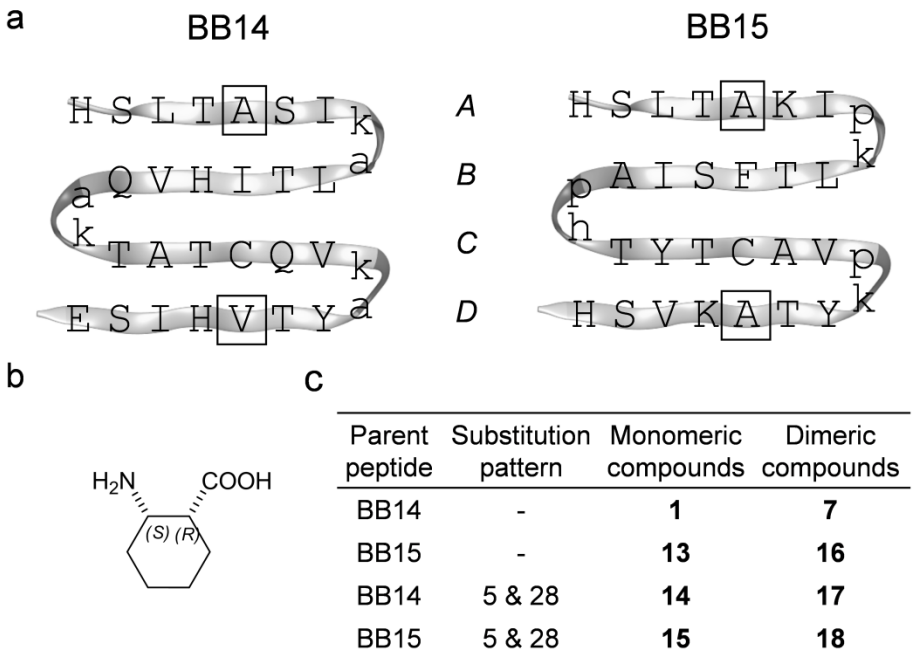

Parent peptide	Substitution pattern	Monomeric compounds	Dimeric compounds
BB14	-	**1**	**7**
BB15	-	**13**	**16**
BB14	5 & 28	**14**	**17**
BB15	5 & 28	**15**	**18**

Figure 17. Amino acid sequence and secondary structure representation of model betabellin structures (**a**) and ACHC-analogs. The residues are coded with standard one-letter α-amino acid notations; lower-case letters indicate D-α-amino acids. Squares represent the positions of peripheral *cis*-ACHC replacements. The structure of *cis*-(1*R*,2*S*)-ACHC (**b**). Investigated monomeric and dimeric compounds (**c**).

For this work, we chose and synthesized another member of the betabellin family, BB-15 (**13** and **16**, Figure 17), which was shown to form long fibrils via edge-to-edge aggregation in dimeric form and was proposed as a useful model for studying and inhibiting fibril formation.[8] We intended to keep BB-14 as a control sequence to observe the effect of edge mutations on stability in a system, which is not prone to aggregation. We applied *cis*-(1*R*,2*S*)-ACHC (Figure 17b) mutations at the center of the two peripheral strands (strand A and D), at positions 5 and 28. The 32-residue monomeric and 64-residue disulfide-linked dimeric betabellins and their analogs (Figure 17c) were synthetized and studied.

4.2.2. Dimerization-induced β-sheet formation

First, we investigated the overall folding propensity of the betabellins and their α/β-peptidic analogs using CD spectroscopy. The β-sheet structure of the parent betabellin peptide **1** was already apparent from the CD curve in its monomeric form (Figure 18a).

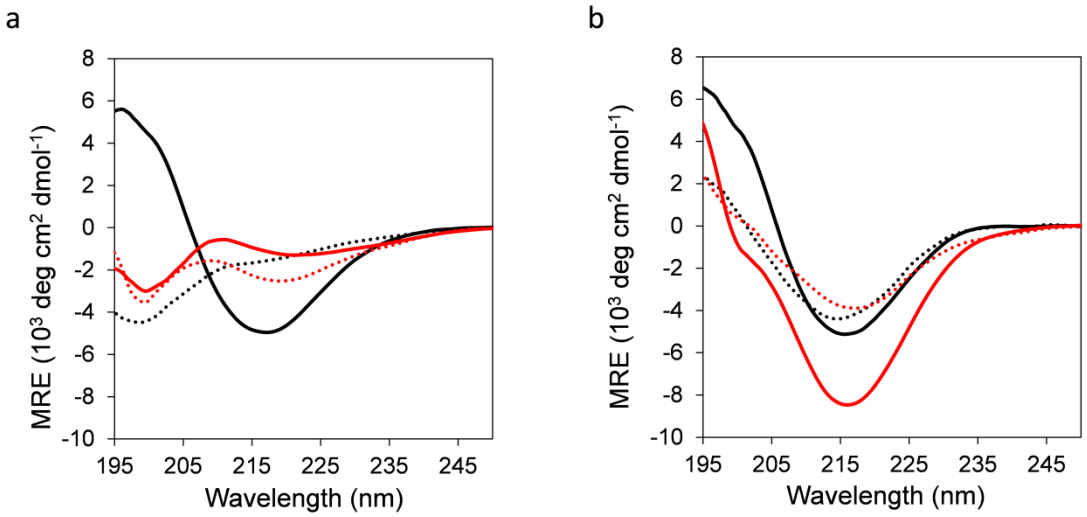

Figure 18. a) Mean residue ellipticities (MRE) obtained for monomeric BB-14 (**1**), BB-15 (**13**) and their ACHC-analogs **14** and **15** indicated in black, red, black dotted and red dotted respectively. b) Mean residue ellipticities (MRE) obtained for dimeric BB-14 (**7**), BB-15 (**16**) and their ACHC-analogs **17** and **18** indicated in black, red, black dotted, and red dotted respectively.

In contrast, **13** and the ACHC-substituted analogs **14** and **15** exhibited U-shaped CD curves with a negative band at approximately 199 nm, suggesting the prevalence of disordered conformations. In accordance with our previous results obtained for the core-mutated betabellin-14 derivatives, the characteristic negative band of the β-sheet appeared at 216 nm for the dimeric compounds (Figure 18b). This indicates dimerization-induced β-sheet folding for template **16** and the edge-substituted derivatives **17** and **18**. As seen before, the formation of **7** via dimerization had little effect on the CD intensity indicating an inherently stable β-sheet. Among the dimeric sequences, **16** displayed the highest intensity at 216 nm, which may indicate increased β-sheet content and/or an altered overall folding pattern. To test the residue-level folding propensities of the dimeric β-sandwiches, NMR experiments were run.

Heteronuclear NMR spectra were recorded and assigned for the dimeric sequences in natural abundance under optimized conditions (HEPES buffer, 500 μM, 298 K). Homonuclear TOCSY and NOESY spectra were used to assign H_α chemical shifts, whereas heteronuclear ^{13}C and HSQC spectra were applied to assign C_α and C_β chemical shifts. ^{13}C HSQC was measured in pure D_2O with identical buffer composition in order to assign C_α chemical shifts by eliminating the water signal. Although $^{13}C_\alpha$ resonances are also sensitive to secondary structure, chemical shift analysis was

performed only using the $^{1}H_{\alpha}$ and $^{13}C_{\beta}$ resonances, because line broadening hindered signal assignment for most sequences, especially for the flexible terminal residues. Therefore, to obtain consistent results, $^{13}C_{\alpha}$ signals were omitted from the comparative analysis. Chemical shifts were converted into residue-specific secondary structure propensity (SSP) scores for each residue, which estimate the folding tendency at the given positions.[148] All sequences exhibited negative SSP scores along the sequence, reflecting the overall β-sheet propensity (Figure 19).

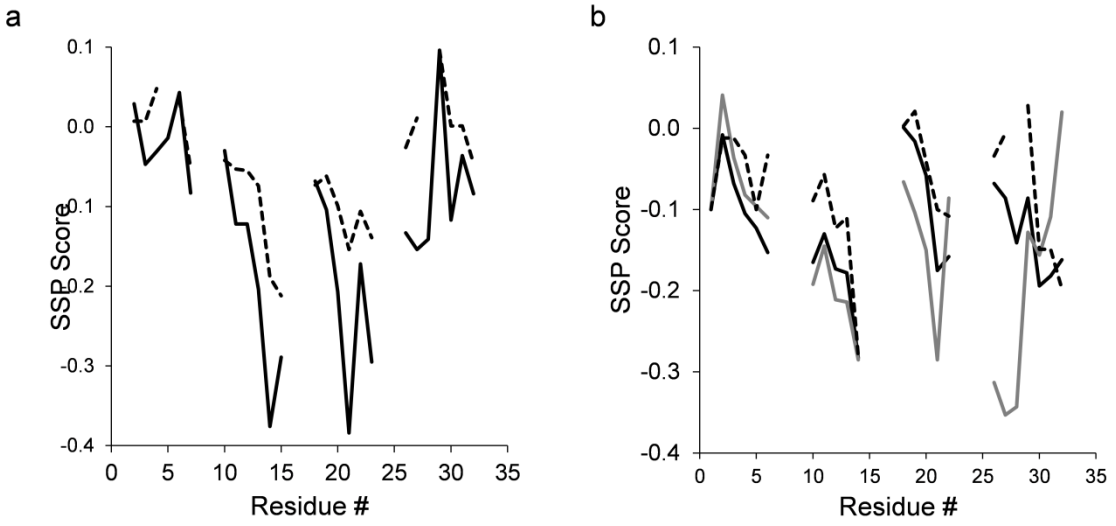

Figure 19. Residue-level secondary structure propensity (SSP) scores calculated via $^{1}H_{\alpha}$ and $^{13}C_{\beta}$ NMR chemical shifts obtained at 298 K. The SSP scores for dimeric betabellins **7** (solid black) and **17** (dashed black) (**a**) and for **16** (solid gray) and **18** (dashed black) (**b**). SSP scores obtained for **16** at 308 K (solid black) are also indicated in panel (**b**). Positive and negative SSP scores indicate regular α-helix and β-sheet formation, respectively.

For the template sequence **7**, the core strands B and C displayed order, while the terminal strands A and D folded only partially into regular β-strand structures. Unexpectedly, the edge mutations in **17** had a marked effect on the folding propensity of the core strands. Despite the limited ability of the edge strands to fold into periodic secondary structures, there were long-range effects on the stability of the internal strands, supporting the view that the β-sandwich core made stabilizing shielding contacts with the more solvent-exposed edge strands without their regular folding. A similar pattern, but a less pronounced effect of the edge mutations, was observed for **16** and **18**. Notably, the core and edge strands displayed a more uniform folding tendency than did **15** and **17**, which can explain the different CD fingerprints. For **16** and **18**,

NOESY contacts were clearly detected between the aromatic and aliphatic side chains supporting the formation of the hydrophobic core, but the spectral quality did not allow the detailed characterization of the backbone contacts. Temperature-dependent CD measurements (see later) suggested that the β-sandwiches of sequences **16**–**18** had higher thermodynamic stability at approximately 308 K; therefore, attempts were made to run NMR experiments at elevated temperatures. Successful assignment was only possible for **16** at 308 K (Figure 19b). We found that temperature stabilized the C-terminal edge strand and that this effect propagated to the β-sandwich core. This result is in accordance with the propensity of **16** for edge-to-edge aggregation and fibril formation.

Similar to the core-substituted compounds, the overlaps in the 2D homonuclear NMR spectra and the residual flexibility of the peptides did not allow atomic-scale resolution in the structural characterization of the compounds.

4.2.3. Thermal and thermodynamic stability

The folding behavior of proteins and protein-mimetic models can be assessed using the thermal denaturation profile. Temperature-dependent CD experiments were acquired (Figure 20a-d), and β-sheet content (MRE_{216}) was plotted against temperature (Figure 20e-f).

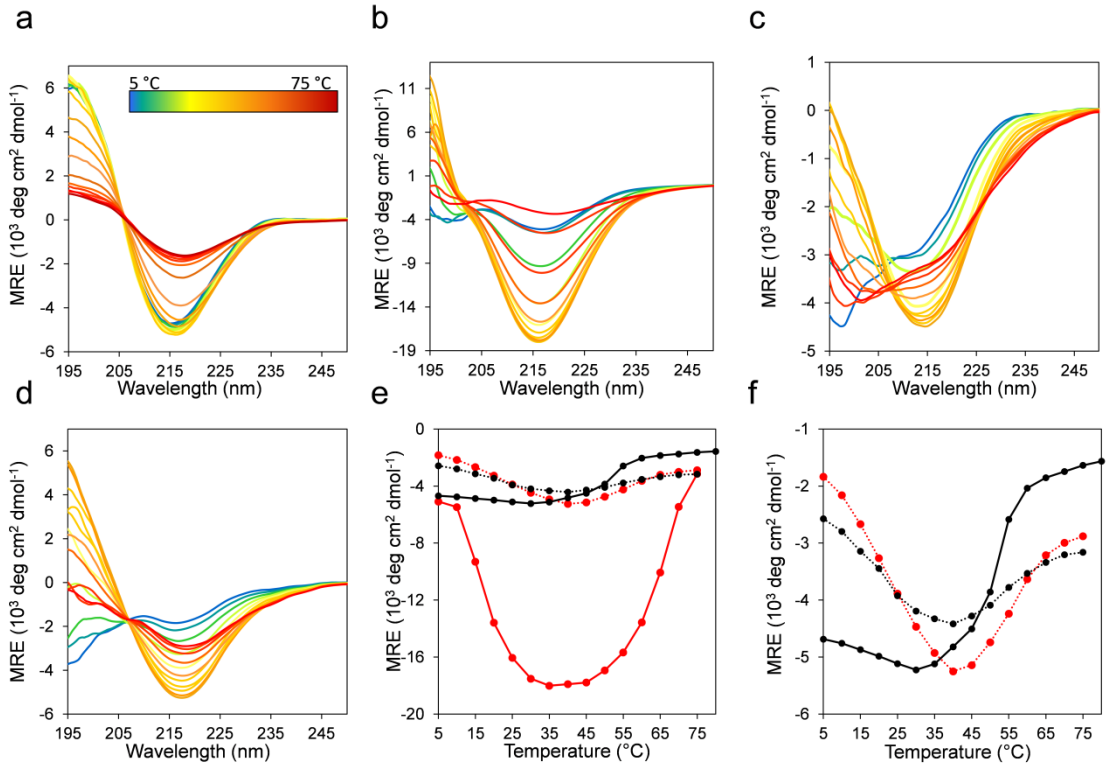

Figure 20. Temperature-dependent CD curves recorded for dimeric betabellins **7** (**a**) and **16** (**b**) and their α/β analogs **17** (**c**) and **18** (**d**). Color code for the temperature scale is given in the inset of panel (**a**). To compare the temperature-dependent β-sheet folding propensity of the compounds, MRE values at 216 nm are plotted as a function of temperature (**e**) and in an enlarged region (**f**) with solid black (**7**), solid red (**16**), dotted black (**17**) and dotted red (**18**).

Structural stability is often described on the basis of only the melting temperature (T_m). A more detailed picture can be obtained upon folding via analysis of the stability curve, which is the free energy of unfolding as a function of temperature. To obtain a set of thermodynamic parameters, the CD-derived temperature-dependent stability data were fitted against a theoretical model described by Privalov[124] as well as Becktel and Schellman.[123] In this model, the temperature-independent heat capacity of unfolding (ΔC_p), the temperature of maximum stability (T_s), and the temperature-independent components of enthalpy (ΔH_s) and entropy (ΔS_s) of unfolding were obtained (Figure 21 and Table 1). The maximum free energy of unfolding (ΔG_s) and the temperatures for cold (T_c) and thermal (T_m) denaturation could also be calculated in the analysis.[121]

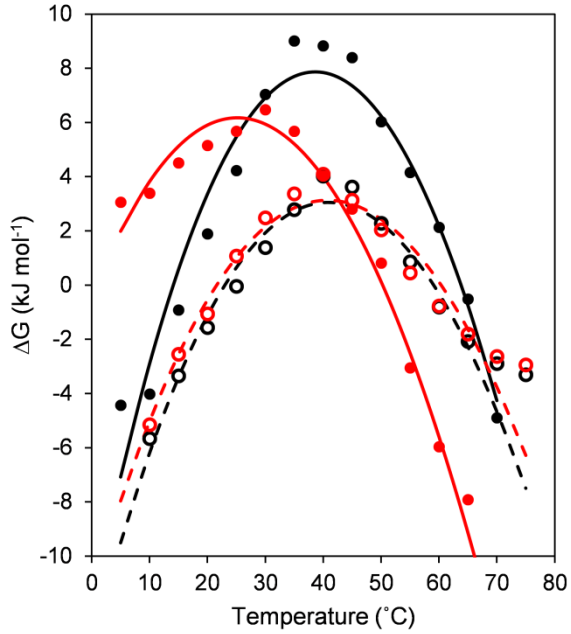

Figure 21. Experimental protein stability curves (free energy of unfolding) for **7** (filled red), **16** (filled black), **17** (empty red) and **18** (empty black). The fit curves are indicated with solid red, solid black, dashed red and dashed black for **7**, **16**, **17** and **18**, respectively.

		7	**16**	**17**	**18**
ΔH_s	kJ mol^{-1}	10.2	11.7	8.3	7.9
ΔS_s	J mol^{-1} K^{-1}	13.6	12.2	16.3	15.5
ΔC_p	kJ mol^{-1} K^{-1}	6.0	7.9	5.2	5.9
ΔG_s	kJ mol^{-1}	6.2	7.9	3.1	3.1
T_s	˚C	25.8	39.1	41.8	41.7
T_c	˚C	0.7	14.1	21.6	23.0
T_m	˚C	50.3	63.8	60.4	59.1

Table 1. Thermodynamic parameters of unfolding obtained from the stability curves.

The temperature-dependent CD experiments revealed protein-like denaturation behavior for all β-sandwich mimetics, where both thermal and cold denaturations were observed. This curvature of the stability curve is a result of positive ΔC_p, which is strongly connected to the solvent-mediated cooperative unfolding transition via disruption of manifold of weak interactions and solvation of the polar and non-polar groups.[150, 151] The edge ACHC replacements uniformly decreased the maximum stabilities (ΔG_s) for the α/β sequences, but this loss of thermodynamic stability still

affords maximum folded populations above 82% for both **17** and **18**. On the other hand, the edge ACHC replacements in **17** shifted T_s to a considerably higher temperature, which led to a marked increase in thermal stability and the appearance of cold denaturation at room temperature. Sequences **16** and **18** displayed only a small difference in T_s, whereas room-temperature cold denaturation was also observed for **18**. Cold denaturation occurs through the effective solvation of apolar side chains by water at low temperatures. This process can be promoted by the frustrated electrostatic interactions and the increased solvent accessibility of the hydrophobic core (trapped water). As the modeling results for **10** showed, the H-bond network and back-bone curvature around the ACHC residue are geometrically distorted, which certainly increase the solvent accessibility in the folded state. This is in line with the NMR findings of this work. The ΔC_p per-residue value for the unfolding of native proteins is in the range 42–84 J mol^{-1} K^{-1},[152] and it is increased by the percentage of the buried non-polar surface and the satisfied H-bonds in the folded state. Betabellins are designed to have a high ratio of buried non-polar side chains, and thus the parent sequences displayed ΔC_p per-residue values of 93.8 and 124.0 J mol^{-1} for **7** and **16**, respectively. The cyclic β-amino acid mutations changed these per-residue-based values to 81.7 and 92.0 J mol^{-1} for **17** and **18**, respectively, which are still native protein-like figures despite their bulging geometry and frustrated H-bonds around the ACHC residues. This finding indicated that the hydrophobic effect is an important stabilizing factor, which is facilitated by an irregular edge region that contacts the core region. Accordingly, the edge strands were able to convey stabilizing contacts to the core, as detected by NMR. A large weight of the hydrophobic effect in the overall stability of the α/β sequences can explain the good thermal stability of **17** and **18**. The temperature-independent parts of the enthalpy and entropy values are determined by a complex interplay between structural features and enthalpy–entropy compensation that is encoded in the protein sequence itself, which makes the assignment of a single factor to the changes difficult. However, it is notable that ΔS_s increased upon ACHC replacements, pointing to an entropically favored unfolding of the α/β sequences, which again can be a sign of extra local rigidity induced by the cyclic β-residues with a possible contribution by the trapped water in the folded state. However, the less stable H-bonds in the folded states

of **17** and **18** might be reflected in their less endothermic unfolding compared to **7** and **16**. These β-residue-induced changes in the thermodynamics of β-sandwich folding are the opposite of those observed for protein helix segments.

4.2.4. Stability against edge-to-edge aggregation

We tested the ability of the altered terminal strand geometry to inhibit salt-induced edge-to-edge aggregation and fibril formation, using **16** and **18** as models. The experiments above were performed under NaCl-free conditions to maintain **16** in monomeric form and to facilitate the detection of stability changes upon α → β substitutions. Diffusion-ordered NMR spectroscopy measurements under low-salt conditions recorded for **16** and **18** did not indicate any significant differences in the sizes or shapes of the NMR-visible fraction of the peptides. The presence of NaCl scales up the hydrophobic effects, acting both as a β-sandwich stabilizing factor and a promoter of aggregation in the following experiments.

At elevated salt concentrations (above 40 mM NaCl), a significant intensity loss was observed in the NMR spectra of **16** (Figure 22a), likely due to the immediate formation of high-molecular-weight associates with extreme short transversal relaxation. In contrast, the NMR-visible fraction of α/β-analog **18** did not display a marked decrease, even at physiological salt concentration (Figure 22b). These results indicated that the aggregation of the α/β sequence is not induced at near-physiological salt concentrations. At a NaCl concentration of 120 mM, only 15% of the parent fibril-forming betabellin **16** remained in the NMR-visible form, in contrast with the 93% of **18** (Figure 22c). In terms of the stability against aggregation at physiological NaCl concentrations, ACHC-substituted analog **18** proved to be more stable than **16**. To further support the behavior concerning edge-to-edge association, TEM images of the samples with high salt content were recorded. In line with the literature results, NaCl triggered the aggregation of **16**, and long thin fibrils were observed with an approximate size of 3.5 nm × 400 nm (Figure 22d), whereas no visible aggregates were found in the sample containing α/β-analog **18** (Figure 22e).

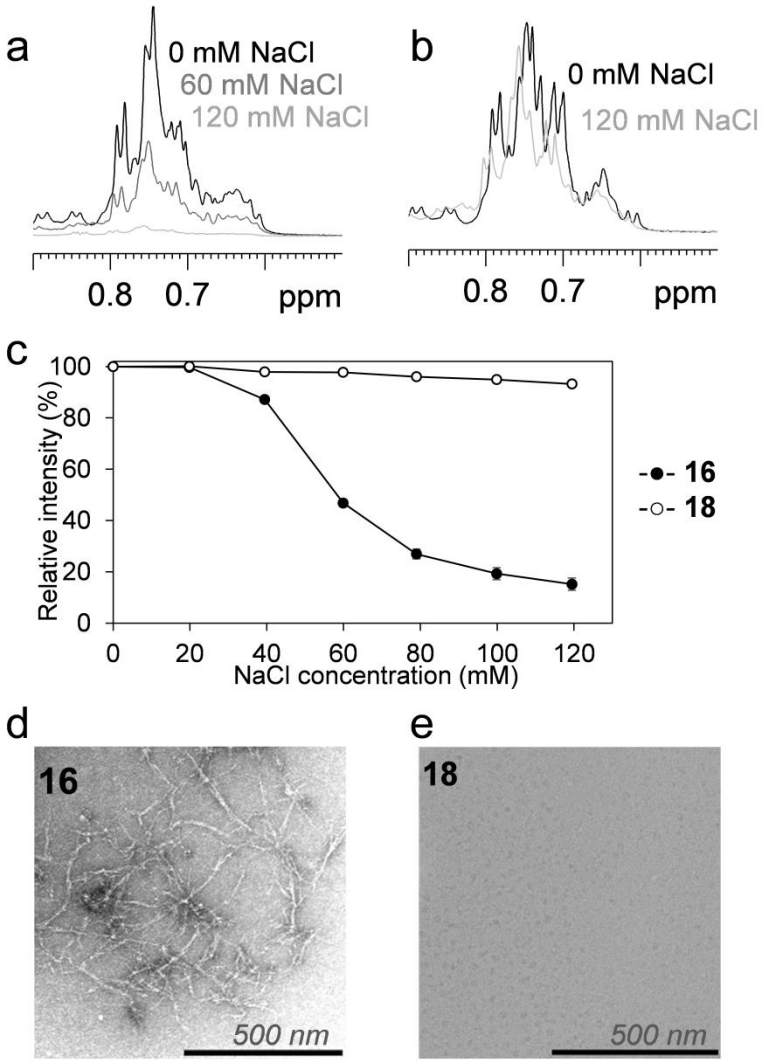

Figure 22. Reduced fibrillization tendency of **18** compared to **16**. The methyl region of the ^{1}H NMR spectra of **16** and **18** at increasing NaCl concentrations (**a** and **b**, respectively). The NMR-visible fraction of the peptides assessed by the integration of ^{1}H NMR signals at various NaCl concentrations (**c**). Integrals were carefully corrected for dilution effects and the possible salt-dependent sensitivity loss of the NMR probe. The TEM images of **16** and **18** are given in panels (**d**) and (**e**), respectively.

4.3. Conclusions

The design of β-sheet-containing tertiary structure mimetics is a current challenge in protein engineering, because β-sheets are key elements in many protein–protein interactions. Only a few protein-sized foldameric structures have been reported in the literature, and none of them investigated the β-sandwich fold. We selected a *de novo* designed β-sandwich model protein, betabellin-14 as template and introduced β-amino acids with different steric and conformational properties to study the effect of β-residue

mutations on the hydrophobic core. We found that the hydrophobic core is very sensitive to mutations, thus the analogs displayed reduced folding propensity. However, dimerization through disulfide bond enhanced β-sheet formation in a way similar to the parent betabellin sequence. We observed that the nature of the β-residues determined the folding propensity and residual flexibility of the chains. Both the fit into the local β-sheet conformational environment with high hydrogen-bonding engagement and the steric fit into the hydrophobic core are essential for the maintenance of β-sheet content and rigidity to obtain protein-like behavior. We found that (1*R*,2*S*)-ACHC, selected in accord with the stereochemical patterning principle, met both these requirements simultaneously acceptably well, and was therefore unique among the β-amino acid building blocks studied. In contrast, other β-residues either disrupted the hydrophobic core, or introduced a conformational mismatch relative to ACHC. Overall, we have shown the feasibility of β-amino acid mutations in the hydrophobic core of the β-sandwich tertiary fold and found a residue, (1*R*,2*S*)-ACHC, which may be of general use in the design of β-sheet mimetics.

Uncontrolled aggregation is a general obstacle in the design of protein drugs, and structures with high β-sheet content are the most prone to self-association. We observed that while the *cis*-ACHC residue fits into the β-sheet environment, the additional carbon atom in the backbone introduced a bulge in the strand, which is a feature of several natural edge-protection strategies. We designed and synthesized analogs of betabellin-14 and the fibril-forming betabellin-15 with peripheral *cis*-ACHC mutations to utilize this as protection against edge-to-edge aggregation end to study thermal and thermodynamic stability. Protein-like folding behavior was observed for all compounds studied, and higher β-sheet content was achieved compared to core substitution. The irregularity at the peripheral strands promoted by *cis*-ACHC replacements decreased thermodynamic stability, but the temperatures of maximum stability were either increased to or maintained at 40 °C, not far from physiological temperatures. In terms of sensitivity to aggregation, the irregular peripheral strands were effective as edge protection and successfully tuned down the unfavorable aggregation propensity of BB-15 at physiological salt concentration. In contrast with common strategies, edge protection was achieved without interfering with the side-chain orientation, the

electrostatic pattern of the H-bond pillars or the net charge. Overall, we conclude that *cis*-ACHC replacements at open edges can maintain sufficient thermodynamic stability to facilitate a predominant β-sandwich tertiary structure, provide favorable thermal stability profiles and offer an effective control over unwanted aggregation, with the potential benefit of contributing to protease resistance.

5. Summary

1. In order to investigate the feasibility and the rules of β-amino acid replacements in a protein-sized β-sandwich scaffold, we designed and synthesized seven foldameric analogs of two betabellin model proteins, betabellin-14 and betabellin-15, containing β-amino acids, in 32-residue monomeric and in 64-residue dimeric forms.
   1.1. The first design strategy involved substitution of core hydrophobic residues in betabellin-14 with homologous β^3-amino acids and with different conformationally constrained cyclic β-residues.
   1.2. In the second part of the work we introduced cyclic β-amino acid substitutions in the peripheral strands of betabellin-14 and betabellin-15 to investigate the effects on stability and edge-to-edge aggregation.
2. Overall folding behavior of the foldamers was analyzed by CD.
   2.1. Dimerization-induced folding similar to the parent sequences was observed for all analogs except **12** containing bulky ABHC residues.
   2.2. Deconvolution of the CD spectra was carried out for a quantitative estimation of the secondary structural content, revealing differences in the induced β-sheet contents of the analogs. All foldamers exhibited less ordered structure compared to the parent sequence. The highest β-sheet content was achieved with 1*R*,2*S*-aminocyclohexanecarboxylic acid (ACHC) substitutions.
   2.3. Compared to core mutations, peripheral substitutions resulted in higher overall β-sheet content.
3. Temperature-dependent CD measurements were carried out to investigate the stability and cooperativity of the folding.
   3.1. Protein-like cold and thermal denaturations were observed in the parent sequences and the analogs containing ACHC residues.
   3.2. The stability curve of the peripheral-substituted compounds was calculated from the CD data and compared to those of the parent sequences, revealing a decrease in the thermodynamic stability, but not in the temperature of maximum stability.

4. NMR spectroscopic experiments were run and secondary chemical shift analysis was performed to obtain residue-level structural data.
    4.1. The chemical shifts of all compounds could be successfully assigned and SSP scores were calculated.
    4.2. A local distortion of the structure was observed around the β-residues.
    4.3. Dimerization induced the β-sheet content mostly in the strand containing the Cys residue, propagating to the other strands. The induced β-sheet content was the highest for analog **10**, while other analogs showed varying folding behaviors and a lower extent of inducibility.
    4.4. Peripheral mutations also had a marked effect on the folding propensity of the core strands, suggesting the presence of shielding contacts between the edge and core strands.
5. Molecular dynamics calculations were performed to gain information on the side-chain-dependent folding behavior.
    5.1. In line with the experimental data, the simulations predicted **10** as the most rigid among the α/β analogs, as well as having the smallest deviation from the structure of the parent sequence.
    5.2. We analyzed the solvent-accessible surface of the hydrophobic core and the number of backbone H-bonds as markers of compact folding, and found that **10** displayed values closest to BB-14. The lack of cooperative folding observed for the other analogs could be explained either with insufficient fitting into the hydrophobic core (**8** and **12**) or a conformational mismatch disrupting the H-bond network (**9** and **11**).
6. NMR and TEM measurements were employed to study the aggregation properties under high salt concentrations. The parent BB-15 sequence was found to form fibrils, but no aggregation was observed for **18**, suggesting that peripheral ACHC-substitution is an efficient method to prevent edge-to-edge association.

Acknowledgements

This work was carried out in the Institute of Pharmaceutical Chemistry during the years 2011–2014 and in the Institute of Pharmaceutical Analysis, University of Szeged during the years 2014–2018.

I would like to express my deep gratitude to my supervisor Prof Dr. Tamás Martinek, Head of the Institute of Pharmaceutical Analysis 2014–2018, for his guidance to complete this work, his inspiring ideas and constructive suggestions**.**

I owe my thanks to Dr. Edit Wéber and Dr. Anasztázia Hetényi for performing the NMR measurements and helping me when any difficulties arose.

I would like to thank Lukács Németh for his help in setting up the molecular dynamics simulations and in their evaluation, and Dr. Lívia Fülöp and Titanilla Szögi for helping with the TEM measurements.

I am grateful to Dr. István Mándity for providing insights to peptide synthetic methods and to Prof. Dr. Ferenc Fülöp head of the Institute of Pharmaceutical Chemistry 1998–2017 for providing me with the possibility to carry out part of my work in the institute.

I am grateful to all my colleagues in the Department of Pharmaceutical Analysis and Pharmaceutical Chemistry for their help and useful advice.

I wish to express my warmest thanks to my family and friends for their encouragement and understanding during my PhD studies.

References

1. S. H. Gellman, *Accounts of chemical research*, 1998, **31**, 173-180.
2. D. J. Hill, M. J. Mio, R. B. Prince, T. S. Hughes and J. S. Moore, *Chemical Reviews*, 2001, **101**, 3893-4012.
3. D. R. Davies and S. Chacko, *Accounts of chemical research*, 1993, **26**, 421-427.
4. A. M. Watkins and P. S. Arora, *ACS chemical biology*, 2014, DOI: 10.1021/cb500241y.
5. J. T. Ryman and B. Meibohm, *CPT: Pharmacometrics & Systems Pharmacology*, 2017, **6**, 576-588.
6. H. Inouye, J. E. Bond, S. P. Deverin, A. Lim, C. E. Costello and D. A. Kirschner, *Biophys J*, 2002, **83**, 1716-1727.
7. A. Lim, A. M. Makhov, M. J. Saderholm, J. D. Griffith and B. W. Erickson, *Biochem. Biophys. Res. Commun.*, 1999, **264**, 498-504.
8. A. Lim, M. J. Saderholm, A. M. Makhov, M. Kroll, Y. B. Yan, L. Perera, J. D. Griffith and B. W. Erickson, *Protein Sci.*, 1998, **7**, 1545-1554.
9. Y. Yan and B. W. Erickson, *Protein Science*, 1994, **3**, 1069-1073.
10. D. Whitford, *Proteins: Structure and Function*, Wiley, 2005.
11. T. A. Martinek and F. Fulop, *Chemical Society Reviews*, 2012, **41**, 687-702.
12. C. M. Goodman, S. Choi, S. Shandler and W. F. DeGrado, *Nature Chemical Biology*, 2007, **3**, 252.
13. L. K. Pilsl and O. Reiser, *Amino acids*, 2011, **41**, 709-718.
14. W. S. Horne and S. H. Gellman, *Accounts of chemical research*, 2008, **41**, 1399-1408.
15. H. M. Werner and W. S. Horne, *Current opinion in chemical biology*, 2015, **28**, 75-82.
16. G. A. Lengyel, G. A. Eddinger and W. S. Horne, *Org Lett*, 2013, **15**, 944-947.
17. I. M. Mandity, E. Weber, T. A. Martinek, G. Olajos, G. K. Toth, E. Vass and F. Fulop, *Angewandte Chemie International Edition*, 2009, **48**, 2171-2175.
18. I. M. Mandity, L. Fulop, E. Vass, G. K. Toth, T. A. Martinek and F. Fulop, *Org Lett*, 2010, **12**, 5584-5587.
19. J. W. Checco and S. H. Gellman, *Current opinion in structural biology*, 2016, **39**, 96-105.
20. J. A. Kritzer, J. D. Lear, M. E. Hodsdon and A. Schepartz, *J Am Chem Soc*, 2004, **126**, 9468-9469.
21. Ł. Berlicki, L. Pilsl, E. Wéber, I. M. Mándity, C. Cabrele, T. A. Martinek, F. Fülöp and O. Reiser, *Angewandte Chemie International Edition*, 2012, **51**, 2208-2212.
22. R. W. Cheloha, J. A. Sullivan, T. Wang, J. M. Sand, J. Sidney, A. Sette, M. E. Cook, M. Suresh and S. H. Gellman, *ACS chemical biology*, 2015, **10**, 844-854.
23. H. S. Haase, K. J. Peterson-Kaufman, S. K. Lan Levengood, J. W. Checco, W. L. Murphy and S. H. Gellman, *J Am Chem Soc*, 2012, **134**, 7652-7655.
24. J. D. Sadowsky, J. K. Murray, Y. Tomita and S. H. Gellman, *Chembiochem : a European journal of chemical biology*, 2007, **8**, 903-916.
25. D. F. Hook, P. Bindschadler, Y. R. Mahajan, R. Sebesta, P. Kast and D. Seebach, *Chem Biodivers*, 2005, **2**, 591-632.
26. D. Seebach, S. Abele, J. V. Schreiber, B. Martinoni, A. K. Nussbaum, H. Schild, H. Schulz, H. Hennecke, R. Woessner and F. Bitsch, *CHIMIA International Journal for Chemistry*, 1998, **52**, 734-739.
27. H. Wiegand, B. Wirz, A. Schweitzer, G. P. Camenisch, M. I. Rodriguez Perez, G. Gross, R. Woessner, R. Voges, P. I. Arvidsson and J. Frackenpohl, *Biopharmaceutics & drug disposition*, 2002, **23**, 251-262.

28. R. Srinivasan and G. D. Rose, *Proceedings of the National Academy of Sciences*, 1999, **96**, 14258.
29. G. P. Dado and S. H. Gellman, *Journal of the American Chemical Society*, 1994, **116**, 1054-1062.
30. D. H. Appella, L. A. Christianson, D. A. Klein, M. R. Richards, D. R. Powell and S. H. Gellman, *Journal of the American Chemical Society*, 1999, **121**, 7574-7581.
31. D. H. Appella, L. A. Christianson, I. L. Karle, D. R. Powell and S. H. Gellman, *Journal of the American Chemical Society*, 1996, **118**, 13071-13072.
32. J. L. Matthews, K. Gademann, B. Jaun and D. Seebach, *Journal of the Chemical Society, Perkin Transactions 1*, 1998, DOI: 10.1039/A805478I, 3331-3340.
33. K. Gademann, A. Häne, M. Rueping, B. Jaun and D. Seebach, *Angewandte Chemie International Edition*, 2003, **42**, 1534-1537.
34. D. Seebach, K. Gademann, V. Schreiber JüRg, L. Matthews Jennifer, T. Hintermann, B. Jaun, L. Oberer, U. Hommel and H. Widmer, *Helv Chim Acta*, 2004, **80**, 2033-2038.
35. E. Szolnoki, A. Hetenyi, T. A. Martinek, Z. Szakonyi and F. Fulop, *Org Biomol Chem*, 2012, **10**, 255-259.
36. É. Szolnoki, A. Hetényi, I. M. Mándity, F. Fülöp and T. A. Martinek, *European Journal of Organic Chemistry*, 2013, **2013**, 3555-3559.
37. A. Hayen, A. Schmitt Margaret, N. Ngassa Felix, A. Thomasson Kathryn and H. Gellman Samuel, *Angewandte Chemie International Edition*, 2004, **43**, 505-510.
38. C. M. Grison, J. A. Miles, S. Robin, A. J. Wilson and D. J. Aitken, *Angewandte Chemie International Edition*, 2016, **55**, 11096-11100.
39. P. Prabhakaran, S. S. Kale, V. G. Puranik, P. R. Rajamohanan, O. Chetina, J. A. K. Howard, H.-J. Hofmann and G. J. Sanjayan, *Journal of the American Chemical Society*, 2008, **130**, 17743-17754.
40. Y. J. Chung, B. R. Huck, L. A. Christianson, H. E. Stanger, S. Krauthauser, D. R. Powell and S. H. Gellman, *J. Am. Chem. Soc.*, 2000, **122**, 3995-4004.
41. Y. J. Chung, B. R. Huck, L. A. Christianson, H. E. Stanger, S. Krauthauser, D. R. Powell and S. H. Gellman, *J. Am. Chem. Soc.*, 2001, **123**, 5851-5851.
42. D. Seebach, S. Abele, K. Gademann and B. Jaun, *Angewandte Chemie International Edition*, 1999, **38**, 1595-1597.
43. C. R. Jones, M. K. N. Qureshi, F. R. Truscott, S. T. D. Hsu, A. J. Morrison and M. D. Smith, *Angew. Chem. Int. Ed.*, 2008, **47**, 7099-7102.
44. M. Khurram, N. Qureshi and M. D. Smith, *Chem. Commun.*, 2006, DOI: 10.1039/b611882h, 5006-5008.
45. E. Vass, U. Strijowski, K. Wollschläger, I. M. Mándity, G. Szilvágyi, M. Jewgiński, K. Gaus, S. Royo, Z. Majer, N. Sewald and M. Hollósi, *J. Pept. Sci.*, 2010, **16**, 613-620.
46. S. Chandrasekhar, A. Sudhakar, M. U. Kiran, B. N. Babu and B. Jagadeesh, *Tetrahedron Letters*, 2008, **49**, 7368-7371.
47. Z. E. Reinert, G. A. Lengyel and W. S. Horne, *J Am Chem Soc*, 2013, **135**, 12528-12531.
48. Z. Hegedus, E. Weber, E. Kriston-Pal, I. Makra, A. Czibula, E. Monostori and T. A. Martinek, *J. Am. Chem. Soc.*, 2013, **135**, 16578-16584.
49. Z. Hegedus, I. Makra, N. Imre, A. Hetenyi, I. M. Mandity, E. Monostori and T. A. Martinek, *Chemical Communications*, 2016, **52**, 1891-1894.
50. R. Spencer, K. H. Chen, G. Manuel and J. S. Nowick, *European Journal of Organic Chemistry*, 2013, **2013**, 3523-3528.
51. T. L. Raguse, J. R. Lai, P. R. LePlae and S. H. Gellman, *Organic Letters*, 2001, **3**, 3963-3966.

52. R. P. Cheng and W. F. DeGrado, *Journal of the American Chemical Society*, 2002, **124**, 11564-11565.
53. D. S. Daniels, E. J. Petersson, J. X. Qiu and A. Schepartz, *Journal of the American Chemical Society*, 2007, **129**, 1532-1533.
54. W. S. Horne, J. L. Price, J. L. Keck and S. H. Gellman, *Journal of the American Chemical Society*, 2007, **129**, 4178-4180.
55. M. W. Giuliano, W. S. Horne and S. H. Gellman, *Journal of the American Chemical Society*, 2009, **131**, 9860-9861.
56. J. L. Price, W. S. Horne and S. H. Gellman, *Journal of the American Chemical Society*, 2010, **132**, 12378-12387.
57. P. S. P. Wang and A. Schepartz, *Chemical Communications*, 2016, **52**, 7420-7432.
58. R. G. Brennan and B. W. Matthews, *The Journal of biological chemistry*, 1989, **264**, 1903-1906.
59. B.-C. Lee, R. N. Zuckermann and K. A. Dill, *Journal of the American Chemical Society*, 2005, **127**, 10999-11009.
60. N. Delsuc, J.-M. Léger, S. Massip and I. Huc, *Angewandte Chemie International Edition*, 2006, **46**, 214-217.
61. J. L. Price, E. B. Hadley, J. D. Steinkruger and S. H. Gellman, *Angewandte Chemie International Edition*, 2009, **49**, 368-371.
62. V. M. Sharma Gangavaram, V. Subash, K. Narsimulu, R. Sankar Ampapathi and C. Kunwar Ajit, *Angewandte Chemie International Edition*, 2006, **45**, 8207-8210.
63. S. De, B. Chi, T. Granier, T. Qi, V. Maurizot and I. Huc, *Nature chemistry*, 2017, **10**, 51.
64. A. M. Gronenborn, D. R. Filpula, N. Z. Essig, A. Achari, M. Whitlow, P. T. Wingfield and G. M. Clore, *Science*, 1991, **253**, 657.
65. Z. E. Reinert and W. S. Horne, *Chemical Science*, 2014, **5**, 3325-3330.
66. G. A. Lengyel, Z. E. Reinert, B. D. Griffith and W. S. Horne, *Org Biomol Chem*, 2014, **12**, 5375-5381.
67. K. L. George and W. S. Horne, *Journal of the American Chemical Society*, 2017, **139**, 7931-7938.
68. C. Mayer, M. Müller Manuel, H. Gellman Samuel and D. Hilvert, *Angewandte Chemie International Edition*, 2014, **53**, 6978-6981.
69. D. F. Kreitler, D. E. Mortenson, K. T. Forest and S. H. Gellman, *Journal of the American Chemical Society*, 2016, **138**, 6498-6505.
70. J. Garric, J.-M. Léger and I. Huc, *Chemistry – A European Journal*, 2007, **13**, 8454-8462.
71. C. Bao, B. Kauffmann, Q. Gan, K. Srinivas, H. Jiang and I. Huc, *Angewandte Chemie International Edition*, 2008, **47**, 4153-4156.
72. J.-L. Hou, X.-B. Shao, G.-J. Chen, Y.-X. Zhou, X.-K. Jiang and Z.-T. Li, *Journal of the American Chemical Society*, 2004, **126**, 12386-12394.
73. H. Juwarker, J. M. Suk and K. S. Jeong, *Chem Soc Rev*, 2009, **38**, 3316-3325.
74. G. M. Blackburn, *Nucleic Acids in Chemistry and Biology*, Royal Society of Chemistry, Cambridge, UK, 2006.
75. T. Kimmerlin, K. Namoto and D. Seebach, *Helv Chim Acta*, 2003, **86**, 2104-2109.
76. K. Namoto, J. Gardiner, T. Kimmerlin and D. Seebach, *Helv Chim Acta*, 2006, **89**, 3087-3103.
77. S. Müller, K. Laxmi-Reddy, V. Jena Prakrit, B. Baptiste, Z. Dong, F. Godde, T. Ha, R. Rodriguez, S. Balasubramanian and I. Huc, *Chembiochem : a European journal of chemical biology*, 2014, **15**, 2563-2570.

78. V. Kesavan, N. Tamilarasu, H. Cao and T. M. Rana, *Bioconjugate Chemistry*, 2002, **13**, 1171-1175.
79. N. Tamilarasu, I. Huq and T. M. Rana, *Journal of the American Chemical Society*, 1999, **121**, 1597-1598.
80. X. Wang, I. Huq and T. M. Rana, *Journal of the American Chemical Society*, 1997, **119**, 6444-6445.
81. M. A. Gelman, S. Richter, H. Cao, N. Umezawa, S. H. Gellman and T. M. Rana, *Organic Letters*, 2003, **5**, 3563-3565.
82. Y. Hamuro, J. P. Schneider and W. F. DeGrado, *Journal of the American Chemical Society*, 1999, **121**, 12200-12201.
83. D. Liu and W. F. DeGrado, *Journal of the American Chemical Society*, 2001, **123**, 7553-7559.
84. T. L. Raguse, E. A. Porter, B. Weisblum and S. H. Gellman, *J Am Chem Soc*, 2002, **124**, 12774-12785.
85. B. Geueke, K. Namoto, I. Agarkova, J.-C. Perriard, E. Kohler Hans-Peter and D. Seebach, *Chembiochem : a European journal of chemical biology*, 2005, **6**, 982-985.
86. D. Seebach, K. Namoto, R. Mahajan Yogesh , P. Bindschädler, R. Sustmann, M. Kirsch, S. Ryder Neil , M. Weiss, M. Sauer, C. Roth, S. Werner, H.-D. Beer, C. Munding, P. Walde and M. Voser, *Chemistry & Biodiversity*, 2004, **1**, 65-97.
87. N. Umezawa, M. A. Gelman, M. C. Haigis, R. T. Raines and S. H. Gellman, *Journal of the American Chemical Society*, 2002, **124**, 368-369.
88. S. Moreira Irina, A. Fernandes Pedro and J. Ramos Maria, *Proteins: Structure, Function, and Bioinformatics*, 2007, **68**, 803-812.
89. M. R. Arkin and J. A. Wells, *Nature Reviews Drug Discovery*, 2004, **3**, 301.
90. J. A. Kritzer, J. D. Lear, M. E. Hodsdon and A. Schepartz, *Journal of the American Chemical Society*, 2004, **126**, 9468-9469.
91. E. A. Harker, D. S. Daniels, D. A. Guarracino and A. Schepartz, *Bioorganic & Medicinal Chemistry*, 2009, **17**, 2038-2046.
92. E. A. Harker and A. Schepartz, *Chembiochem : a European journal of chemical biology*, 2009, **10**, 990-993.
93. A. D. Bautista, J. S. Appelbaum, C. J. Craig, J. Michel and A. Schepartz, *Journal of the American Chemical Society*, 2010, **132**, 2904-2906.
94. J. P. Plante, T. Burnley, B. Malkova, M. E. Webb, S. L. Warriner, T. A. Edwards and A. J. Wilson, *Chemical Communications*, 2009, DOI: 10.1039/B908207G, 5091-5093.
95. V. Azzarito, J. A. Miles, J. Fisher, T. A. Edwards, S. L. Warriner and A. J. Wilson, *Chemical Science*, 2015, **6**, 2434-2443.
96. T. Hara, S. R. Durell, M. C. Myers and D. H. Appella, *Journal of the American Chemical Society*, 2006, **128**, 1995-2004.
97. J. D. Sadowsky, M. A. Schmitt, H.-S. Lee, N. Umezawa, S. Wang, Y. Tomita and S. H. Gellman, *Journal of the American Chemical Society*, 2005, **127**, 11966-11968.
98. E. F. Lee, J. D. Sadowsky, B. J. Smith, P. E. Czabotar, K. J. Peterson-Kaufman, P. M. Colman, S. H. Gellman and W. D. Fairlie, *Angewandte Chemie International Edition*, 2009, **48**, 4318-4322.
99. M. D. Boersma, H. S. Haase, K. J. Peterson-Kaufman, E. F. Lee, O. B. Clarke, P. M. Colman, B. J. Smith, W. S. Horne, W. D. Fairlie and S. H. Gellman, *Journal of the American Chemical Society*, 2012, **134**, 315-323.
100. W. S. Horne, M. D. Boersma, M. A. Windsor and S. H. Gellman, *Angew Chem Int Ed*, 2008, **47**, 2853-2856.

101. J. W. Checco, E. F. Lee, M. Evangelista, N. J. Sleebs, K. Rogers, A. Pettikiriarachchi, N. J. Kershaw, G. A. Eddinger, D. G. Belair, J. L. Wilson, C. H. Eller, R. T. Raines, W. L. Murphy, B. J. Smith, S. H. Gellman and W. D. Fairlie, *Journal of the American Chemical Society*, 2015, **137**, 11365-11375.
102. O. M. Stephens, S. Kim, B. D. Welch, M. E. Hodsdon, M. S. Kay and A. Schepartz, *Journal of the American Chemical Society*, 2005, **127**, 13126-13127.
103. A. D. Bautista, O. M. Stephens, L. Wang, R. A. Domaoal, K. S. Anderson and A. Schepartz, *Bioorganic & Medicinal Chemistry Letters*, 2009, **19**, 3736-3738.
104. W. S. Horne, L. M. Johnson, T. J. Ketas, P. J. Klasse, M. Lu, J. P. Moore and S. H. Gellman, *Proceedings of the National Academy of Sciences of the United States of America*, 2009, **106**, 14751-14756.
105. L. M. Johnson, D. E. Mortenson, H. G. Yun, W. S. Horne, T. J. Ketas, M. Lu, J. P. Moore and S. H. Gellman, *Journal of the American Chemical Society*, 2012, **134**, 7317-7320.
106. Y. Imamura, N. Watanabe, N. Umezawa, T. Iwatsubo, N. Kato, T. Tomita and T. Higuchi, *Journal of the American Chemical Society*, 2009, **131**, 7353-7359.
107. Y. Imamura, N. Umezawa, S. Osawa, N. Shimada, T. Higo, S. Yokoshima, T. Fukuyama, T. Iwatsubo, N. Kato, T. Tomita and T. Higuchi, *Journal of Medicinal Chemistry*, 2013, **56**, 1443-1454.
108. L. Fülöp, I. M. Mándity, G. Juhász, V. Szegedi, A. Hetényi, E. Wéber, Z. Bozsó, D. Simon, M. Benkő, Z. Király and T. A. Martinek, *PloS one*, 2012, **7**, e39485.
109. R. W. Cheloha, A. Maeda, T. Dean, T. J. Gardella and S. H. Gellman, *Nature biotechnology*, 2014, **32**, 653-655.
110. E. V. Denton, C. J. Craig, R. L. Pongratz, J. S. Appelbaum, A. E. Doerner, A. Narayanan, G. I. Shulman, G. W. Cline and A. Schepartz, *Organic letters*, 2013, **15**, 5318-5321.
111. N. Koglin, C. Zorn, R. Beumer, C. Cabrele, C. Bubert, N. Sewald, O. Reiser and A. G. Beck-Sickinger, *Angewandte Chemie (International ed. in English)*, 2003, **42**, 202-205.
112. Ł. Berlicki, M. Kaske, R. Gutiérrez-Abad, G. Bernhardt, O. Illa, R. M. Ortuño, C. Cabrele, A. Buschauer and O. Reiser, *Journal of Medicinal Chemistry*, 2013, **56**, 8422-8431.
113. K. Gademann, M. Ernst, D. Hoyer and D. Seebach, *Angewandte Chemie International Edition*, 1999, **38**, 1223-1226.
114. T. Yamazaki, A. PrÖBstl, W. Schiller Peter and M. Goodman, *International Journal of Peptide and Protein Research*, 1991, **37**, 364-381.
115. X. Liu, Y. Wang, Y. Xing, J. Yu, H. Ji, M. Kai, Z. Wang, D. Wang, Y. Zhang, D. Zhao and R. Wang, *J Med Chem*, 2013, **56**, 3102-3114.
116. T. P. Quinn, N. B. Tweedy, R. W. Williams, J. S. Richardson and D. C. Richardson, *Proceedings of the National Academy of Sciences of the United States of America*, 1994, **91**, 8747-8751.
117. D. Sanfelice and P. A. Temussi, *Biophys Chem*, 2016, **208**, 4-8.
118. P. Seneci, in *Molecular Targets in Protein Misfolding and Neurodegenerative Disease*, ed. P. Seneci, Academic Press, San Diego, 2015, DOI: https://doi.org/10.1016/B978-0-12-800186-8.00001-8, pp. 1-38.
119. W. Wang, *International journal of pharmaceutics*, 2005, **289**, 1-30.
120. P. Goddard, *Advanced Drug Delivery Reviews*, 1991, **6**, 103-131.
121. D. Sanfelice, E. Morandi, A. Pastore, N. Niccolai and P. A. Temussi, *Chemphyschem*, 2015, **16**, 3599-3602.
122. F. Pucci, M. Dhanani, Y. Dehouck and M. Rooman, *PloS one*, 2014, **9**, e91659.
123. W. J. Becktel and J. A. Schellman, *Biopolymers*, 1987, **26**, 1859-1877.
124. P. L. Privalov, *Thermochim Acta*, 1990, **163**, 33-46.

125. T. Szyperski, J. L Mills, D. Perl and J. Balbach, *Combined NMR-observation of cold denaturation in supercooled water and heat denaturation enables accurate measurement of ΔC p of protein unfolding*, 2006.
126. J. S. Richardson and D. C. Richardson, *Proceedings of the National Academy of Sciences of the United States of America*, 2002, **99**, 2754-2759.
127. P. Craveur, A. P. Joseph, J. Rebehmed and A. G. de Brevern, *Protein science : a publication of the Protein Society*, 2013, **22**, 1366-1378.
128. A. J. Doig, *Chemical Communications*, 1997, **22**, 2153-2154.
129. J. Chatterjee, F. Rechenmacher and H. Kessler, *Angewandte Chemie (International ed. in English)*, 2013, **52**, 254-269.
130. D. Ghosh, P. Lahiri, H. Verma, S. Mukherjee and J. Chatterjee, *Chemical Science*, 2016, **7**, 5212-5218.
131. W. Wang and M. H. Hecht, *Proceedings of the National Academy of Sciences of the United States of America*, 2002, **99**, 2760-2765.
132. J. S. Nowick, E. M. Smith, J. W. Ziller and A. J. Shaka, *Tetrahedron*, 2002, **58**, 727-739.
133. Z. Szakonyi, T. A. Martinek, R. Sillanpää and F. Fülöp, *Tetrahedron: Asymmetry*, 2008, **19**, 2296-2303.
134. J. P. W. Tam, C. R.; Liu W.; Zhang J. W., *A highly selective and effective reagent for disulfide bond formation in peptide synthesisa and protein folding.*, ESCOM Science Publishers, Leiden, The Netherlands, Peptides: Chemistry and biology edn., 1992.
135. A. Perczel, M. Hollosi, G. Tusnady and G. D. Fasman, *Protein engineering*, 1991, **4**, 669-679.
136. A. Perczel, K. Park and G. D. Fasman, *Analytical biochemistry*, 1992, **203**, 83-93.
137. A. Perczel, K. Park and G. D. Fasman, *Proteins*, 1992, **13**, 57-69.
138. D. Wishart, B. Sykes and F. Richards, *Biochemistry*, 1992, **31**, 1647-1651.
139. H. Zhang, S. Neal and D. S. Wishart, *J. Biomol. NMR*, 2003, **25**, 173-195.
140. L. J. Németh, Z. Hegedüs and T. A. Martinek, *Journal of Chemical Information and Modeling*, 2014, DOI: 10.1021/ci5003476, 10.1021/ci5003476.
141. X. Daura, W. F. van Gunsteren and A. E. Mark, *Proteins: Structure, Function & Bioinformatics*, 1999, **34**, 269-280.
142. J. Reed and T. A. Reed, *Analytical biochemistry*, 1997, **254**, 36-40.
143. S. Spera and A. Bax, *Journal of the American Chemical Society*, 1991, **113**, 5490-5492.
144. D. S. Wishart, B. D. Sykes and F. M. Richards, *Journal of molecular biology*, 1991, **222**, 311-333.
145. D. S. Wishart, B. D. Sykes and F. M. Richards, *Biochemistry*, 1992, **31**, 1647-1651.
146. D. S. Wishart and A. M. Nip, *Biochem. Cell. Biol.*, 1998, **76**, 153-163.
147. M. Kjaergaard, S. Brander and F. M. Poulsen, *Journal of biomolecular NMR*, 2011, **49**, 139-149.
148. J. A. Marsh, V. K. Singh, Z. Jia and J. D. Forman-Kay, *Protein Sci.*, 2006, **15**, 2795-2804.
149. A. J. Rader, B. M. Hespenheide, L. A. Kuhn and M. F. Thorpe, *Proc. Natl. Acad. Sci. U. S. A.*, 2002, **99**, 3540-3545.
150. A. Cooper, *Biophys Chem*, 2005, **115**, 89-97.
151. A. Cooper, *Biophys Chem*, 2000, **85**, 25-39.
152. C. Ganesh, N. Eswar, S. Srivastava, C. Ramakrishnan and R. Varadarajan, *FEBS letters*, 1999, **454**, 31-36.

APPENDIX

I

II